JOURNAL OF GEOPHYSICAL RESEARCH, VOL. 112, F02035, doi:10.1029/2006JF000667, 2007

Response of glacial landscapes to spatial variations in rock uplift rate

Simon H. Brocklehurst[1] and Kelin X. Whipple[2]

Received 28 August 2006; revised 16 January 2007; accepted 26 February 2007; published 28 June 2007.

[1] The response of glaciated landscapes to rapid rock uplift, driven by tectonic convergence, is an important, often neglected, aspect of proposed interactions between plate tectonic processes and climate change. Rivers typically respond to more rapid rock uplift in part through increasing channel gradients. In contrast, the ''glacial buzzsaw'' hypothesis suggests that glaciers can erode as quickly as the fastest rock uplift rates (6–10 mm/yr) without any increase in mean elevations. However, it has not been established how this is achieved. We examined moving window maps, swath and longitudinal profiles, hillslope relief, and hypsometry for glacierized and formerly glacierized basins in areas of spatially variable rock uplift rate in the Southern Alps, New Zealand, and around Nanga Parbat, Pakistan, to determine whether glaciers have a specific response to rapid rock uplift. The response of these glaciated landscapes to rapid rock uplift (6–10 mm/yr) comprises (1) modest steepening of the longitudinal profiles in smaller glaciated basins, (2) maintenance of shallow downvalley slopes in larger glaciated basins (>~30 km^2, Southern Alps; >~100 km^2, Nanga Parbat), (3) development of tall headwalls, and (4) steepening of the basin as a whole, dominated by hillslope lengthening. Around Nanga Parbat, headwalls several kilometers high constitute >50% of the basin relief. At rapid rock uplift rates, although glaciers can incise the valley floor swiftly, they cannot prevent headwalls from reaching exceptional heights. The associated increase in mean distance between cirque heads (i.e., a decrease in drainage density) causes regional mean elevation to rise with increasing rock uplift rate. However, this is much less than the changes in elevation expected in unglaciated ranges.

Citation: Brocklehurst, S. H., and K. X. Whipple (2007), Response of glacial landscapes to spatial variations in rock uplift rate, *J. Geophys. Res.*, *112*, F02035, doi:10.1029/2006JF000667.

1. Introduction

[2] The potential for important interactions amongst climate change, tectonics and surface processes has received considerable attention in recent years [e.g., *Beaumont et al.*, 1992; *Beaumont et al.*, 2001; *Bookhagen et al.*, 2005; *Koons*, 1995; *Molnar and England*, 1990; *Raymo and Ruddiman*, 1992; *Willett*, 1999; *Wobus et al.*, 2003; *Zeitler et al.*, 2001]. Rapidly incising gorges coincide with active, deeply exhumed metamorphic massifs in the syntaxes at either end of the Himalayas [e.g., *Zeitler et al.*, 2001]. Geodynamic models that couple the mechanical and thermal response of orogens to erosional exhumation have demonstrated the influence of erosion on orogen dynamics, particle paths and the surface distribution of metamorphic facies [e.g., *Beaumont et al.*, 2001; *Jamieson et al.*, 2002; *Tomkin*, 2007; *Whipple and Meade*, 2004]. Meanwhile, topography importantly influences weather systems, which drive erosion and thus dictate landscape evolution [e.g., *Bookhagen et al.*, 2006, 2005; *Roe et al.*, 2002, 2003] and exhumation [e.g., *Thiede et al.*, 2004]. Since glaciers have been widespread during the Quaternary, and potentially remove mass more efficiently than rivers [e.g., *Hallet et al.*, 1996; *Meigs and Sauber*, 2000; *Tomkin and Braun*, 2002], they may have played a major role in the recent development of active orogens, particularly if the style of erosional exhumation by glaciers differs noticeably from that achieved by rivers.

[3] Of particular importance to investigations that relate tectonics and climate change is the transition from more widespread fluvial landscapes prior to Late Cenozoic cooling to the subsequent development of extensive alpine glaciation. We have previously examined the key distinctions between fluvial and glacial landscapes in the slowly uplifting Sierra Nevada, California [*Brocklehurst and Whipple*, 2002, 2006]. In comparison with expectations for a fluvial landscape, Sierra Nevada glaciers have lowered both valley floors and neighboring ridgelines above the approximate mean Quaternary equilibrium line altitude (ELA) [*Porter*, 1989]. All glaciers clearly widened their valleys to form characteristic U-shaped cross sections [*Harbor*, 1992], but only the largest glaciers incised significantly downvalley of the ELA [*Brocklehurst and Whipple*, 2006].

[1] School of Earth, Atmospheric and Environmental Sciences, University of Manchester, Manchester, UK.
[2] School of Earth and Space Exploration, Arizona State University, Tempe, Arizona, USA.

0148-0227/07/2006JF000667$09.00

Furthermore, the glaciers in the eastern Sierra Nevada have eroded headward, generating minor relief and reorganizing drainage networks [*Brocklehurst*, 2002; *Brocklehurst and Whipple*, 2002]. *Oskin and Burbank* [2005] have observed similar processes of cirque retreat in the Kyrgyz Range.

[4] The "glacial buzzsaw" hypothesis states that regional mean elevations are limited to a level closely related to the regional ELA. *Brozovic et al.* [1997] first posed this hypothesis from observations that different regions around Nanga Parbat, Pakistan, have similar hypsometry (frequency distribution of elevations), with a peak at the ELA, despite widely varying rock uplift rates (from ~2 to ~8mm/yr). The lack of significant variations in the landscape, despite the differences in rock uplift rate, suggests that the glaciers that dominate the Nanga Parbat region erode at rates comparable to some of the fastest rock uplift rates on the globe without a commensurate increase in either valley slope or glacier accumulation area (landscape area above the ELA). *Mitchell and Montgomery* [2006] found strong relationships between spatial gradients in the ELA of the Cascade Range, and various measures of its morphology, again supporting the buzzsaw hypothesis.

[5] *Brozovic et al.* [1997] included an important caveat to the buzzsaw hypothesis, that localized peaks, such as Nanga Parbat, may penetrate the envelope of elevations close to the ELA to reach much higher elevations. Such generation of spectacular relief may allow peaks to exceed 8 km in elevation even though crustal strength limits mean elevations to at most 5 km [e.g., *Molnar and Lyon-Caen*, 1988]. *Anderson* [2005] also noted the importance of these "teflon peaks", and speculated that they result from a combination of efficient valley erosion by glaciers, and inefficient erosion of igneous intrusive rocks by periglacial processes acting on the neighboring hillslopes, for example under permanent freezing conditions.

[6] While the Himalayas and the Southern Alps have proven to be attractive field sites for numerical studies of the coupling between surface and tectonic processes, most of the surface processes models employed have focused on fluvial and diffusive processes as the major erosive agents [e.g., *Beaumont et al.*, 1992; *Beaumont et al.*, 2001; *Koons*, 1995; *Willett*, 1999]. This reflects the extra complexity associated with incorporating glacial erosion into a landscape evolution model [e.g., *Braun et al.*, 1999; *MacGregor et al.*, 2000; *Tomkin and Braun*, 2002]. For example, *Willett* [1999] models a cross section through the Aoraki/Mt Cook region of the Southern Alps (Figure 1a) with a surface processes model whose only component is fluvial incision. This approach is appropriate when other processes are coupled to stream elevations, but this is not necessarily the case for the landslides, avalanches, rockfall and especially glacial erosion that are clearly active in the Southern Alps [*Augustinus*, 1995; *Hales and Roering*, 2005; *Hovius et al.*, 1997; *Korup*, 2006; *Porter*, 1975]. This does not undermine the main insights of *Willett*'s [1999] study, but it may diminish the relevance of the Southern Alps as a comparison for fluvial model results.

[7] Our study was motivated by the observation that the glacial buzzsaw hypothesis is not completely appropriate in the Southern Alps. As shown in Figure 1, mean elevation rises in association with interpreted rock uplift rates around Aoraki/Mt Cook, while the ELA is at a much more uniform level across the region [*Porter*, 1975]. Therefore we undertook a detailed study (i.e., at the drainage basin scale) of glacial landscape response to tectonics. We sought to examine how the response of glaciers to rapid rates of rock uplift compares with our expectations for fluvial landscapes, and the implications of this for the dynamics of a developing orogen as climate changes. We consider how alpine landscapes in areas of rapid rock uplift have responded to the onset of Late Cenozoic glaciation, and test the "glacial buzzsaw" hypothesis proposed by *Brozovic et al.* [1997]. We also assess the importance of incorporating glacial erosion when modeling the dynamics of active mountain belts [*Tomkin*, 2007].

2. Background: Landscape Response to Rock Uplift

[8] We follow *England and Molnar* [1990] in making a careful distinction between exhumation (the movement of a given package of rocks with respect to the Earth's surface), rock uplift (the movement of a given package of rocks with respect to a reference level such as the geoid) and surface uplift (the movement of the Earth's surface with respect to a reference level such as the geoid). It is exhumation that is readily measured using thermochronologic techniques (barring complications due to particle trajectories and thermal evolution), but it is the more elusive rock uplift that may cause a response in surface processes. Where exhumation and rock uplift are equal, surface uplift is nil, implying topographic steady state (mean elevation invariant in time). A given mountain range may lie anywhere within the spectrum from erosion exceeding rock uplift (declining elevations), through erosion matching rock uplift (mean elevation invariant in time, i.e. topographic steady state), to surface uplift equal to rock uplift (negligible erosion). In the analysis presented below, we do not make assumptions about a steady state balance between rock uplift and erosion. We do, however, assume that the modern topography reflects the response of surface processes to spatially variable erosion rates recorded as exhumation rates by low-temperature thermochronometers, and that the patterns of exhumation rate variation broadly reflect patterns in rock uplift rate. Given that the first-order behavior of glaciers in regions of rapid rock uplift is not yet known, the discussion that follows is generally restricted to the vertical components of rock uplift and erosion.

[9] The response of rivers to changes in rock uplift rate is well understood, at least in qualitative terms. Relief evolution in fluvial environments is most strongly dependent on the response of the bedrock channel system [*Whipple et al.*, 1999]. Concave longitudinal profiles in fluvial landscapes all over the world can usually be described using a power law relationship between local stream gradient, S, and drainage area, A, where the constant is typically called the steepness index, k_s, and the exponent the concavity index, θ [e.g., *Flint*, 1974]:

$$S = k_s A^{-\theta} \quad (1)$$

Several studies have shown that, in general, the concavity index, θ, is insensitive to rock uplift rate, whereas the steepness index, k_s (where appropriately normalized to a

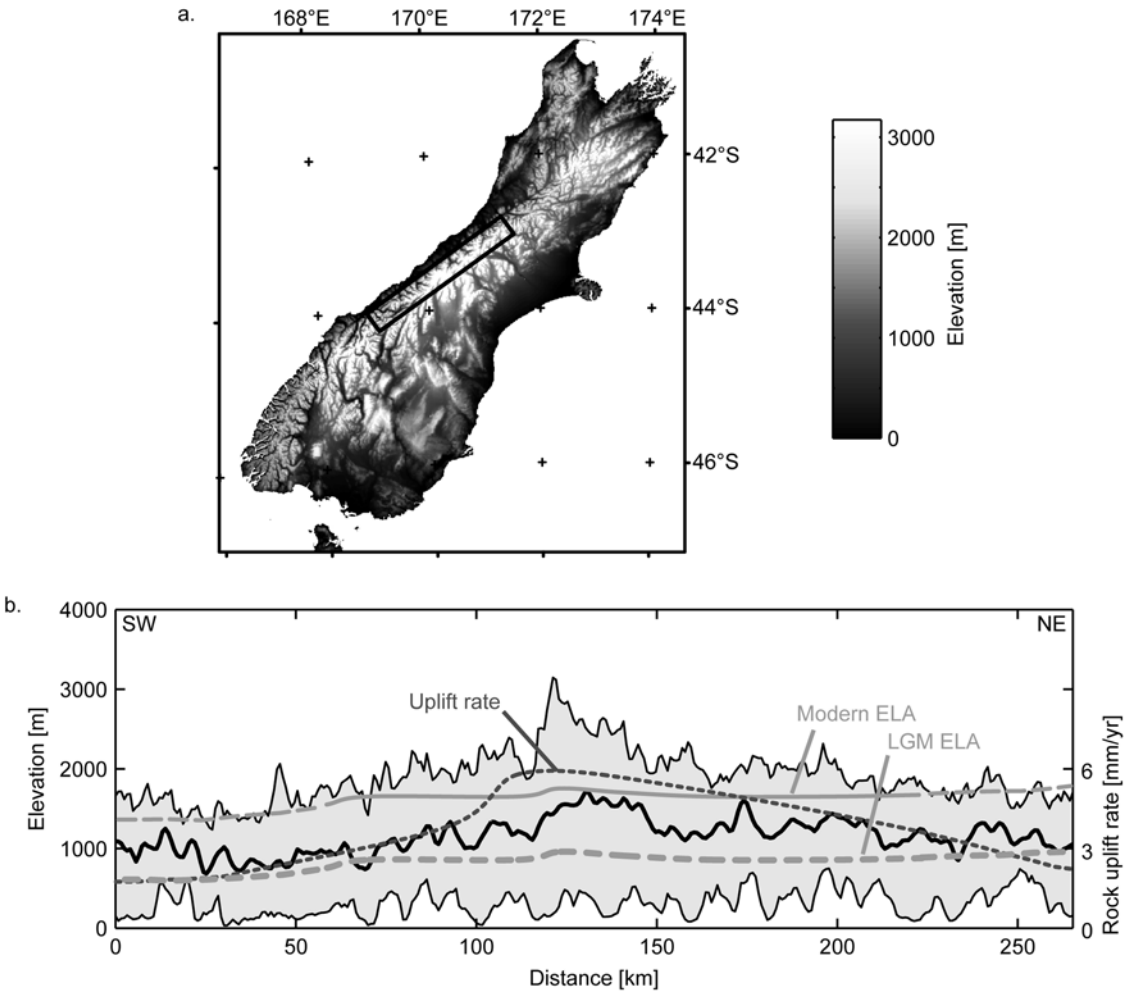

Figure 1. Topographic swath profile along the crest of the Southern Alps, New Zealand. (a) The 1 km GTOPO30 digital topographic data, showing the location of the swath profile in Figure 1b, parallel to the strike of the Southern Alps. Aoraki/Mt Cook lies close to the center of the profile. (b) Maximum (upper thin black curve), mean (thick black curve), and minimum (lower thin black curve) topography along the swath illustrated in Figure 1a, modern (solid gray curve) and Last Glacial Maximum (dashed gray curve) equilibrium line altitudes, and rock uplift rate pattern (dark gray dashed curve). Equilibrium line altitude data from *Porter* [1975]. Exhumation rate data from *Tippett and Kamp* [1993]. The rise in mean elevation associated with more rapid exhumation (and inferred more rapid rock uplift) suggests that the "glacial buzzsaw hypothesis" is not appropriate in this setting.

regional reference concavity index), has a strong, positive correlation with independent measures of rock uplift rate [e.g., *Kobor and Roering*, 2004; *Lague and Davy*, 2003; *Snyder et al.*, 2000; *Whipple*, 2004; *Wobus et al.*, 2006]. Much remains to be established about the physical processes that underlie the relationship between channel steepness and rock uplift rate. However, the key observation relevant to the present study is the fact that at the drainage basin scale, fluvial landscapes respond to higher rock uplift rates by steepening channel gradients throughout the network and thus increasing relief [e.g., *Whipple et al.*, 1999; *Wobus et al.*, 2006].

[11] Hillslope relief is also an important component of drainage basin morphology, and responds to rock uplift through changes in mean gradient or length (and hence drainage density). It is generally accepted that landsliding is the dominant agent of hillslope erosion in a high-relief, tectonically active setting [e.g., *Hewitt*, 1998; *Hovius et al.*, 1997]. *Burbank et al.* [1996] found that hillslope angles in the Nanga Parbat region are largely independent of rock uplift rates, whether glacial or fluvial erosion controls the lower boundary condition for the hillslope. The uniformly high mean slopes suggest a common threshold, namely the stability threshold for bedrock landsliding. This is modeled by assuming that there exists a threshold hillslope gradient, S_h, below which the mass movement rate is negligible, and above which the transport rate becomes effectively infinite [e.g., *Burbank et al.*, 1996; *Densmore et al.*, 1998; *Howard et al.*, 1994; *Tucker and Slingerland*, 1994].

[12] From (1), the expected relationship between drainage density and threshold hillslope for bedrock river channels can be explained as follows [*Howard*, 1997; *Tucker and Bras*, 1998; *Tucker and Whipple*, 2002]. Substituting the threshold hillslope angle for landsliding, S_h, in (1) and

solving for the area of a zero-order catchment, A_0, at which the required channel slope equals the maximum hillslope gradient:

$$A_0 = \left(\frac{k_s}{S_h}\right)^{\frac{1}{\theta}} \quad (2)$$

Since A_0 varies directly with channel steepness, k_s, areas with steeper fluvial catchments should have a lower drainage density (greater channel initiation area). This inverse relation between relief and drainage density is supported by data from the badlands of the western United States [*Howard*, 1997], and from the northern Japanese Alps [*Oguchi*, 1997]. We are not aware of comparable studies of the response of drainage density to rock uplift in glacial landscapes.

[13] *Merrand and Hallet* [2000] and *Braun et al.* [1999] made the first attempts to couple a glacial landscape evolution model with adjustable tectonic uplift. The 1-D *Merrand and Hallet* [2000] model includes seasonal evolution of glacier mass balance, basal hydrology and thermal regime, bedrock erosion, and sediment accumulation and subsequent remobilization. When applied to glaciers of the Chugach–St. Elias Range, Alaska, specific patterns of tectonic forcing are required to sustain the topography necessary to maintain large glaciers over long timescales. This suggests complex coupling between tectonic and surface processes in glacial settings. The 2-D *Braun et al.* [1999] model combines large-scale fluvial erosion, hillslope processes, glacial erosion and generic uniform rock uplift. Though some of the glacial erosion parameters are poorly constrained, they achieve long-term steady state between rock uplift and glacial erosion. Further developments of this model have demonstrated that the presence of basal freezing is a major influence on the relief of tectonically active mountain ranges [*Tomkin and Braun*, 2002], and that there is an important feedback relationship between rock uplift rate and ice mass oscillation [*Tomkin*, 2003].

3. Field Areas

[14] To test the effect of spatial variations in rock uplift rate on glaciated landscapes, we sought glaciated mountain ranges where strong spatial gradients in exhumation rate have been convincingly argued as reflecting gradients in rock uplift rate. Furthermore, in the ideal case, other geomorphic factors, such as climate and lithology, would be held roughly constant.

3.1. New Zealand

[15] *Tippett and Kamp* [1993] obtained a comprehensive suite of apatite and zircon fission track samples for the 300-km-long central section of the Southern Alps. They estimated preuplift paleotemperatures of apatites from each sample by comparing measured values of fission track age and mean length with data relating these variables to temperature in deep hydrocarbon well sections in the Otway Basin, Australia. To move from cooling ages (reflecting exhumation) to rock uplift rates, *Tippett and Kamp* [1993] assumed a normal preuplift geothermal gradient of 27.5 ± 2.5°C/km in the region that became the Southern Alps, and, having shown that the initial mean elevation here was close to sea level, the amount of rock uplift was estimated for each sample. A trend surface of cooling ages from a subset of the data was then used to calculate rock uplift rates. Subsequent criticism of *Tippett and Kamp*'s [1993] work notes that they neglected the role of lateral motion in the thermal conditions experienced by a rock traversing the orogen [e.g., *Batt and Braun*, 1999], and has questioned the zircon partial annealing zone temperatures used [*Walcott*, 1998]. Despite these criticisms, *Tippett and Kamp*'s [1993] interpretation of the post 5 Ma history remains essentially unchanged, and it is this time period that is of interest here in considering the role of Late Cenozoic glaciers in sculpting the modern landscape. *Little et al.* [2005] supplemented the existing data set with hornblende Ar-Ar dating. They delineated a ~20-km-long by 5-km-wide zone north of Fox Glacier and Aoraki/Mt Cook which contains the only hornblendes with alpine total gas ages (i.e., <6Ma). With a revised preuplift geothermal gradient of 20°C/km [*Kamp*, 1997], and a hornblende closure temperate of 550°C, *Little et al.* [2005] calculated an exhumation rate of ~6–9 mm/yr in this zone. *Little et al.* [2005] infer that this maximum in exhumation rate occurs because the Alpine Fault steepens in this region. Either a steepening of the Alpine Fault in the near surface, or an increase in dip-slip rates in the past several million years, would mean contemporary rock uplift rates could be higher than this exhumation rate [*Little et al.*, 2005].

[16] The variation in rock uplift perpendicular to the strike of the range is debated. *Tippett and Kamp* [1993] favor the most rapid rock uplift occurring at the Alpine Fault, *Batt et al.* [2000] prefer uniform rates across a 10–20-km-wide zone adjacent to the fault, *Adams* [1980] envisions maximum rock uplift rates some 7 km southeast of the fault, and *Little et al.* [2005] attributed their "inverted" age trend toward the Alpine Fault to reverse-slip ductile shearing across a zone of distributed deformation extending ~2 km beyond the ~1-km-thick basal mylonite zone. In the context of this study, focused on the northwest side of the main divide of the Southern Alps, the along-strike variations in (vertical) rock uplift rate are more important than the subtleties of variations perpendicular to the strike. We plot rock uplift rates (e.g., Figure 1b) from *Tippett and Kamp* [1993] along a transect ~10 km from the Alpine Fault, accepting that these may underestimate recent rock uplift rates [*Little et al.*, 2005]. Uncertainties associated with the plotted rates reflect both the calculations involved (as described above), and their application over the scale of the basins studied. However, the uncertainties are systematic, and the pattern of rock uplift rate variation is robust. This portion of the Southern Alps is composed almost exclusively of the alpine schist [e.g., *Mason*, 1962]. The glacial history of the Southern Alps has been summarized by *Suggate* [1990], with modern and LGM (Otira glaciation) ELAs determined by *Porter* [1975].

3.2. Pakistan

[17] *Zeitler* [1985] was the first to report extremely young fission track and $^{40}Ar/^{39}Ar$ cooling ages from the Nanga Parbat region, documenting a zone of young ages associated with the Nanga Parbat-Haramosh Massif (NPHM), with older ages to either side (Figure 2b). He obtained exhumation rates from paired apatite and zircon fission track ages

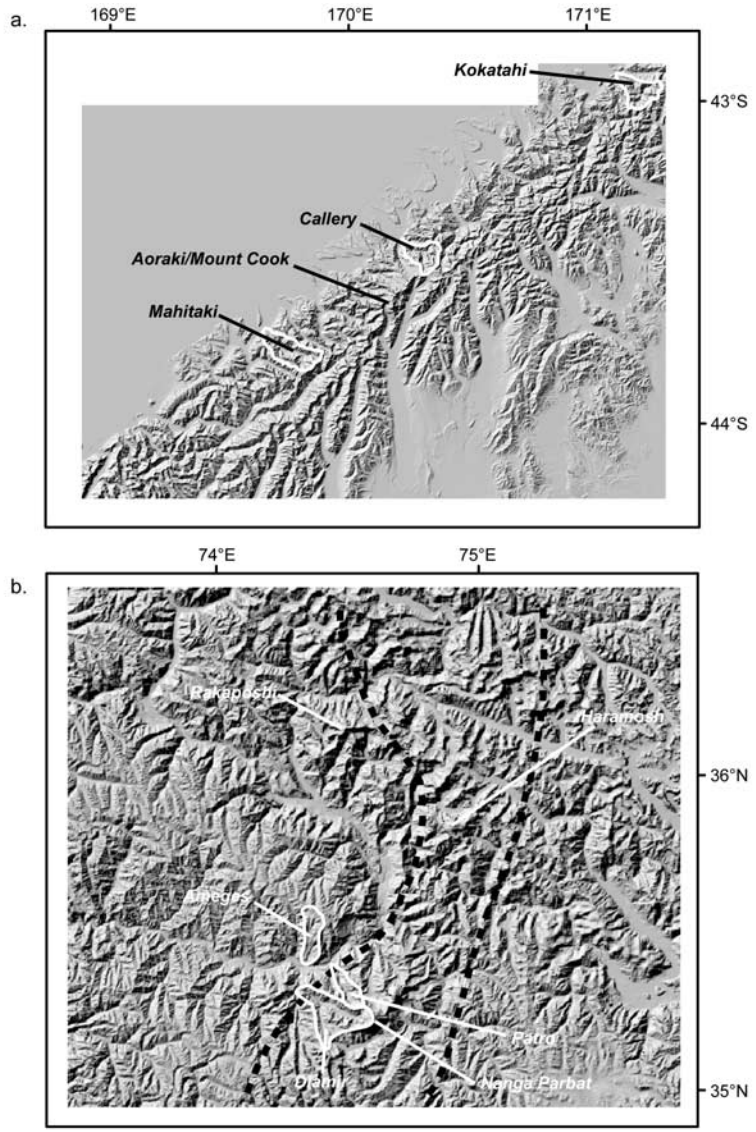

Figure 2. Shaded relief maps of the study areas. (a) Southern Alps. Rock uplift rates are highest in the Aoraki/Mt Cook area (Figure 1b). The Callery, Kokatahi, and Mahitaki basins highlighted are examined in more detail in Figures 3, 5, and 6. (b) Nanga Parbat region. Rapid rock uplift zone from *Zeitler* [1985] is bounded by black dashed curves. The Ameges, Diamir, and Patro basins highlighted are examined in more detail in Figures 3 and 5.

and an assumed geothermal gradient, obtaining rates exceeding 0.5 mm/yr only within the NPHM. *Burbank et al.* [1996] also interpreted *Zeitler*'s [1985] fission track ages in terms of exhumation rates, although they assumed conservative bounds for the geothermal gradient and treated apatite and zircon data independently. Their calculated rates peak at 4–10 mm/yr for apatite, and 2–4 mm/yr for zircon, in the localized area of rapid exhumation along the NPHM (Figure 2b). Exhumation is slower (<2 mm/yr) to either side of this zone. *Gardner and Jones* [1993] examined sediment yields to calculate rates of glacial erosion of 4–6 mm/yr for the Raikot glacier on the northern side of the Nanga Parbat massif, while *Burbank et al.* [1996] used ^{10}Be and ^{26}Al exposure age dating of strath terraces to calculate incision rates of 2–12 mm/yr for the Indus River where it cuts across the Nanga Parbat massif, north of the peak. This correspondence between short-term incision rates and long-term exhumation rates suggests that both record something close to the rock uplift rate. *Burbank et al.* [1996] argue for climatically driven accelerated erosion (exhumation) rates during the Pleistocene. The associated surface lowering means that these exhumation rates may slightly overestimate rock uplift rates. However, this is probably a minor effect, and in any case the spatial pattern of rock uplift/exhumation rate variation remains robust.

[18] The center of the Nanga Parbat massif comprises mostly leucogranites, some with cooling ages as young as 1–10 Ma, again indicative of rapid exhumation, while the surrounding terranes include a variety of metasedimentary gneisses and orthogneisses [e.g., *Schneider et al.*, 1999]. Both the maximum extent and timing of glaciations in the Nanga Parbat region remain controversial [e.g., *Phillips et*

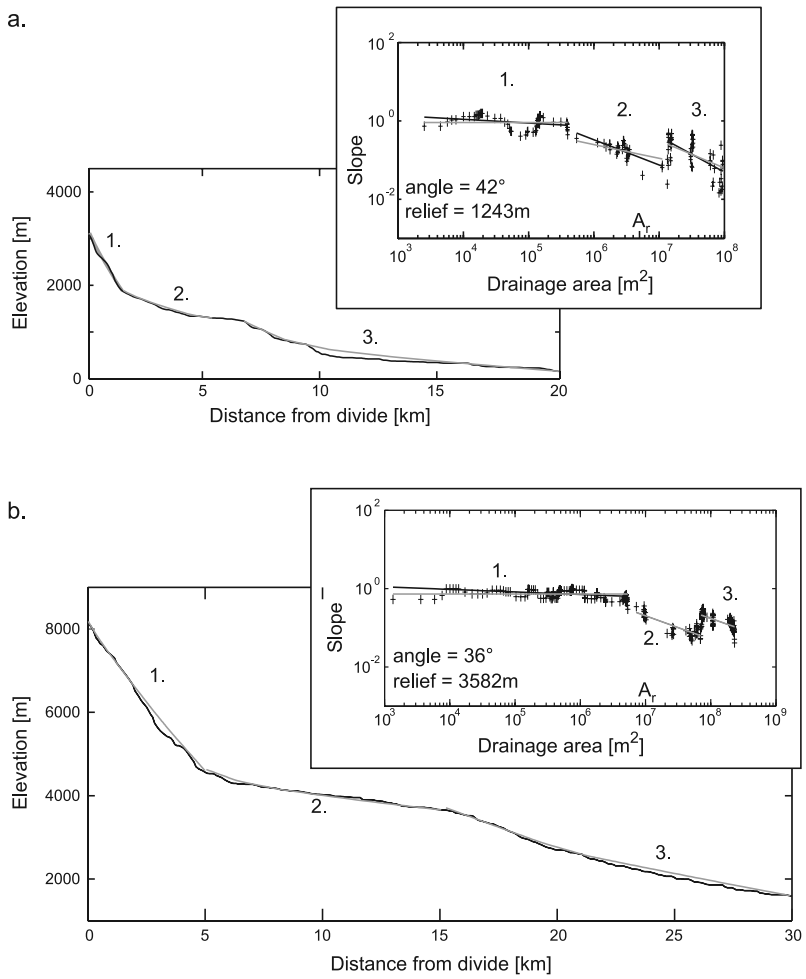

Figure 3. Longitudinal profiles of (a) the Callery River, Southern Alps, and (b) the Diamir Basin, Nanga Parbat. Labels (1), (2), and (3) highlight the three zones of distinct concavity values, $\theta \sim 0$ (hillslope), $\theta \sim 0.4$ (glacier-dominated reach), and $\theta \sim 0.7$ (river-influenced reach), respectively. Main figure shows the longitudinal profile extracted from the digital elevation model (black curve) and the model fits for each section (gray curve). The sections are identified using the slope-area data (inset). On inset graph, black curves are best-fit linear regressions, and gray curves are linear regressions with fixed θ values of 0, 0.4, and 0.7 for zones (1), (2), and (3), respectively.

al., 2000; *Richards et al.*, 2000, 2001], but most studies agree that the largest glaciers extended into the Indus Valley adjacent to Nanga Parbat at their maximum Pleistocene extent [e.g., *Owen et al.*, 2000].

[19] In the discussion that follows, we assume that in both field areas the gradients in exhumation rate can be interpreted as gradients in rock uplift rate. Some surface uplift may have occurred, but this must be minor, because the exhumation rates are so rapid that rocks at the surface today have been elevated from sea level in less than 1 Ma. We therefore refer only to rock uplift rate variations.

4. Methods

[20] The key to our examination of the effects of rock uplift rate on glaciated valleys was to compare drainage basins experiencing different rock uplift rates, while as many other potentially influencing factors (climate, lithology, etc.) as possible remain essentially uniform. We employed five measures of surface topography to analyze the two glaciated mountain ranges: mean elevation and relief maps, swath profiles, hypsometry, valley floor steepness, and hillslope gradient and relief. Except for the maps and swath profiles, we applied each of these approaches to a range of drainage basins of different sizes and rock uplift rates in each range, using 50 m resolution data for the Southern Alps (Land Information New Zealand), and ~90 m resolution data for the Nanga Parbat region, described by *Fielding et al.* [1994]. We examined 55 drainage basins in the Southern Alps (Figure 2a), all on the western side of the drainage divide, and 59 in the Nanga Parbat region (Figure 2b). Drainage basins in the Southern Alps were picked from the range front at the Alpine Fault. We ignored drainage basins with major longitudinal components (e.g., Landsborough River), which may retain topographic signatures of a history on the other side of the divide [e.g., *Craw et al.*, 2003], are substantially larger, and are subject to different precipitation, rock fabric, and tectonic conditions from transverse drainages. In the Nanga Parbat region, drainage

basins were extracted from their junctions with the Indus, Gilgit, Hunza and Astor Rivers. The digital elevation models (DEMs) that we use define the surfaces of any ice present, rather than the elevations of bedrock beneath this ice. Determining the thickness of glaciers is a major undertaking typically requiring ground-penetrating radar or shallow seismic profiling. This data limitation clearly introduces error, since we are seeking to study the (bedrock) landforms of these environments. However, the observation that basal shear stress beneath temperate glaciers

$$\tau_b = \rho g h S' \tag{3}$$

(where τ_b is the basal shear stress, ρ is the ice density, g is acceleration due to gravity, h is the ice thickness, and S' is the surface slope of the ice) is $\sim 0.8-1 \times 10^5$ Pa [e.g., *Paterson*, 1994], implies that it is only in the largest basins with shallowest slopes that there is substantial ice thickness. Given that $\rho g \sim 10^4$, $h \sim 10/S'$, so estimated ice thicknesses for the Callery and Diamir basins (Figure 3) are $\sim$360 m and $\sim$140 m respectively. The ice surface serves mainly to provide a smooth representation of the underlying bedrock, therefore our measurements of downvalley gradient are not substantially affected. Furthermore, the areal extent of ice is modest, so the impact on hypsometry and mean elevation maps is modest. Finally, the ice thickness is a modest fraction of the total relief in these drainage basins, so the effects on headwall relief, swath topography and relief maps are small. We note that in each case our calculations of (bedrock) relief will be underestimates. For our headwall relief measurements, cirque ice may be thicker than surface slopes suggest, again contributing to underestimation of relief. The principle conclusions of this study are therefore not affected by the presence of ice.

4.1. Mean Elevation and Relief Maps and Swath Profiles

[21] We generated a series of maps moving circular windows across the 50m DEM of the Southern Alps. For radii of 1 km and 3 km, we determined elevation range (difference between maximum and minimum elevations) and mean elevation within the moving window. We also extracted swath profiles of maximum, mean and minimum elevation across both field areas, using GTOPO30 1 km digital topographic data (Figures 1 and 4).

4.2. Hypsometry

[22] We employed two approaches to examine the hypsometry, opting to study individual drainage basins rather than arbitrary portions of the landscape [see *Brocklehurst and Whipple*, 2004], namely (1) a *histogram* of the frequencies in different elevation bins (Figures 5a and 5c); and (2) a normalized *cumulative frequency* of the area above a given elevation plotted against elevation (Figures 5b and 5d) [e.g., *Strahler*, 1952]. Both the histogram and cumulative frequency were employed by *Brozovic et al.* [1997].

4.3. Longitudinal Profiles

[23] We extracted longitudinal profiles for the trunk stream (working upstream from the outlet, following the stream with maximum discharge at each confluence) in each drainage basin. Glacial longitudinal profiles are generally characterized by a series of steps and overdeepenings [e.g., *Benn and Evans*, 1998; *Brocklehurst and Whipple*, 2002; *Brocklehurst and Whipple*, 2006; *Hooke*, 1991; *MacGregor et al.*, 2000; *Sugden and John*, 1976]. We found that over longer reaches, and through examining the ice surface rather than the bedrock, these steps were smoothed out, and the glacial longitudinal profiles could be characterized by three distinct zones (see Figure 3): (1) a constant gradient hillslope ($\theta = 0$), (2) a low-concavity middle section in the zone most frequently occupied by ice ($\theta \sim 0.4$), and (3) a more concave lower section ($\theta \sim 0.7$), which we infer displays far greater fluvial influence. The long, shallow middle sections associated with the largest glaciers are particularly striking. Given the concavity of these glacial longitudinal profiles, we use (1) to quantitatively describe their morphology and compare glacial longitudinal profile steepness. However, this is only in the spirit of *Flint*'s [1974] observation that this reasonably describes concave profiles. We do not require that these landscapes are at steady state, nor do we suggest that either k_s or θ relate to processes of glacial erosion. Although the channel steepness index, k_s, is not directly comparable between fluvial and glaciated environments, it still provides a useful metric of the relative downvalley gradients of glacially sculpted valley floors within the study area. We calculated steepness values for the low-concavity ($\theta \sim 0.4$), glacially dominated reach, between the cirque headwall above and the more concave fluvially influenced reach below (Figure 3), to evaluate how much glacial valley profiles steepen in response to increased rock uplift rate. Since k_s and θ determined from regression of slope-area data are correlated, we used the reference slope, S_r, to compare slope in basins with differing concavities [*Sklar and Dietrich*, 1998]. S_r is calculated using the steepness and concavity of a given basin profile, with a single reference drainage area, A_r, that is kept the same across all basins studied, and chosen to lie in the middle of the range of data (see Figure 3).

$$S_r = k_s A_r^{-\theta} \tag{4}$$

The S_r metric is highly correlated to the normalized steepness index, k_{sn}, often used in studies of nonglaciated areas [e.g., *Kirby et al.*, 2003; *Wobus et al.*, 2006], but is more appropriate where a regional reference concavity index is not readily defined.

4.4. Hillslope Relief

[24] We used three different approaches to understand hillslope relief in these glaciated mountain ranges. The first is based on the longitudinal profile, where the hillslope portion is generally linear ($\theta = 0$), having near-constant downslope gradient. The extent of the hillslope is most readily identified in slope-area space, where it is the region of uniform gradient at low drainage areas (Figure 3). We used the slope-area data to calculate the mean slope and the longitudinal profile to determine the vertical relief of the hillslope, for the flow line descending from the highest point on the basin perimeter, because this gives rise to the greatest relief. This metric is herein termed the "headwall relief". In the Southern Alps, we excluded 4 drainage basins from our headwall relief analyses because they have

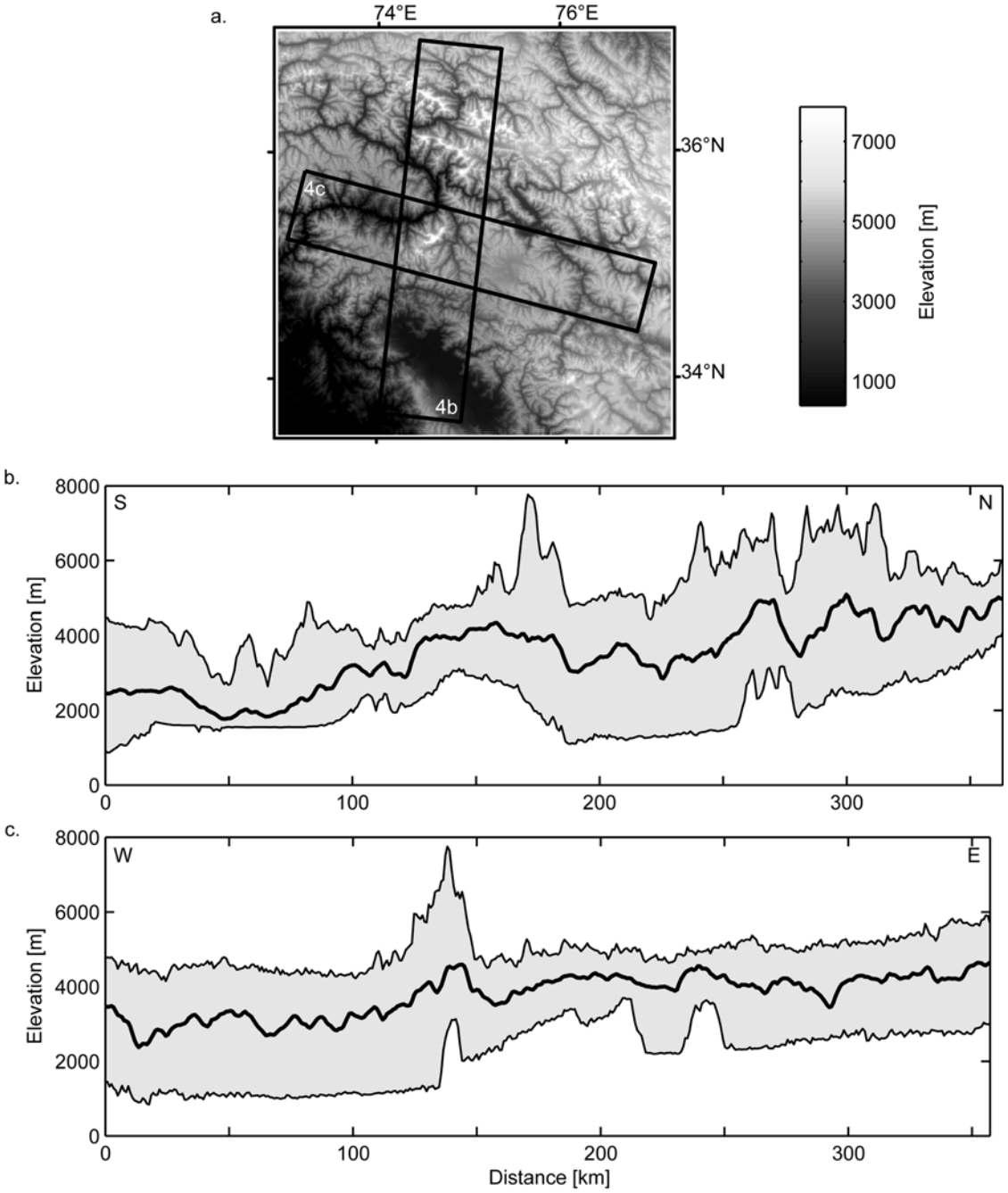

Figure 4. Topographic swath profiles along and across the Nanga Parbat-Haramosh axis. (a) The 1 km GTOPO30 digital topographic data, showing the location of the swath profiles in Figures 4b and 4c. Nanga Parbat lies close to the center of both profiles. (b) Maximum, mean (thick black curve), and minimum topography from south to north along the Nanga Parbat-Haramosh axis, as illustrated in Figure 4a. (c) Swath profile from west to east, across the Nanga Parbat-Haramosh axis; key as in Figure 4b.

ice caps at the drainage divide obscuring much of the headwall.

[25] The second approach draws on the subridgeline relief method [*Brocklehurst and Whipple*, 2002] to look at the distribution of relief across the cirque (Figure 6). We identified the point on the cirque floor/ice surface at the base of the hillslope descending from the highest point in the basin, and used a flow-routing algorithm to isolate only the points in the basin draining to this point on the cirque floor. We then extracted "subridgeline relief" values for all of these points from the subridgeline relief of the whole basin (Figure 6b), and determined the total "missing volume" in the cirque and the corresponding mean subridgeline relief (see discussion by *Brocklehurst and Whipple* [2002]). An alternative would have been to look at the subridgeline relief of the entire cirque, but especially given the presence of ice in many of these drainage basins, we found the base of the hillslope much easier to define consistently (on the basis of a break in slope) than the cirque outlet.

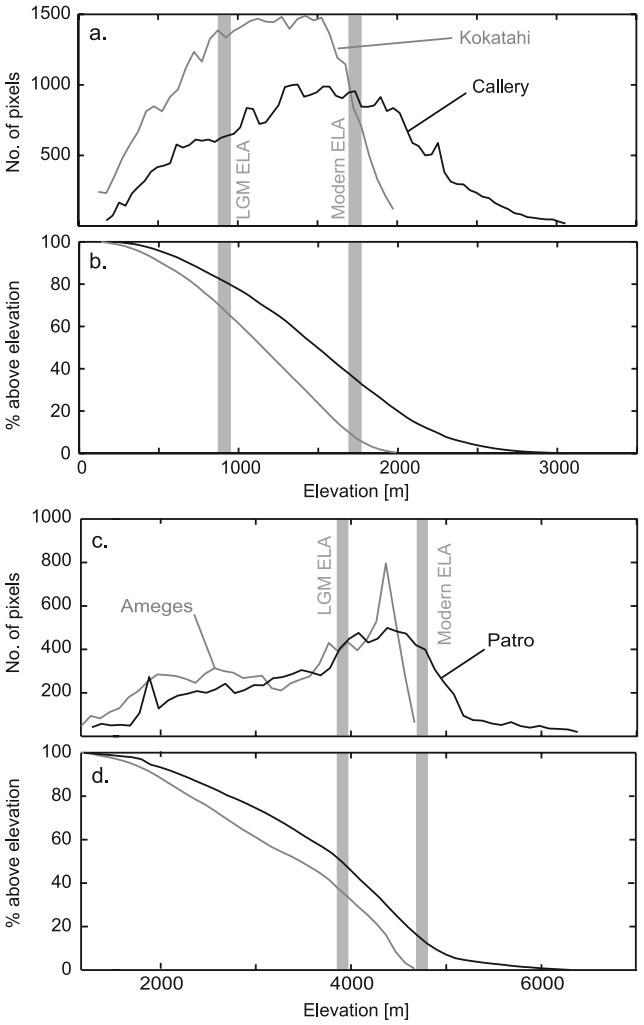

Figure 5. Hypsometry of the Kokatahi (gray curve: slower uplift) and Callery (black curve: faster uplift) river basins, Southern Alps, and Ameges (gray curve: slower uplift) and Patro (black curve: faster uplift) basins, Nanga Parbat region. (a) Frequency distribution of elevations, Southern Alps. Equilibrium line altitude (ELA) estimates from *Porter* [1975]. (b) Cumulative frequency plot, Southern Alps. The Callery Basin is steeper as a whole than the Kokatahi. (c) Frequency distribution of elevations, Nanga Parbat. (d) Cumulative frequency plot, Nanga Parbat. ELA estimates from *Holmes* [1993]. The frequency distribution for the Patro highlights the hillslopes at the top of the basin. These are not areally extensive, but add significantly to the relief of the basin. The cumulative plot suggests that the Patro is slightly steeper than the Ameges, and again highlights the extra relief due to the hillslopes.

[26] The final approach examines the relief of all points along the ridgeline for the subbasin draining to the point on the cirque floor below the highest point in the basin, discussed above. We recognize that in some cases the DEM only indicates the ice surface in the cirque. We isolated all points on the rim of this subbasin (Figure 6c), and for each subtracted the elevation of the pour point on the cirque floor to leave the height above the cirque floor (i.e., relief) of each point on the rim, the "rim relief". Some of these points on the rim are true drainage divides, whereas others just lie on a line descending from the ridgeline to the cirque floor, an artifact of how the subbasin is isolated. To focus on the ridgelines, we noted that the ridgelines tend to

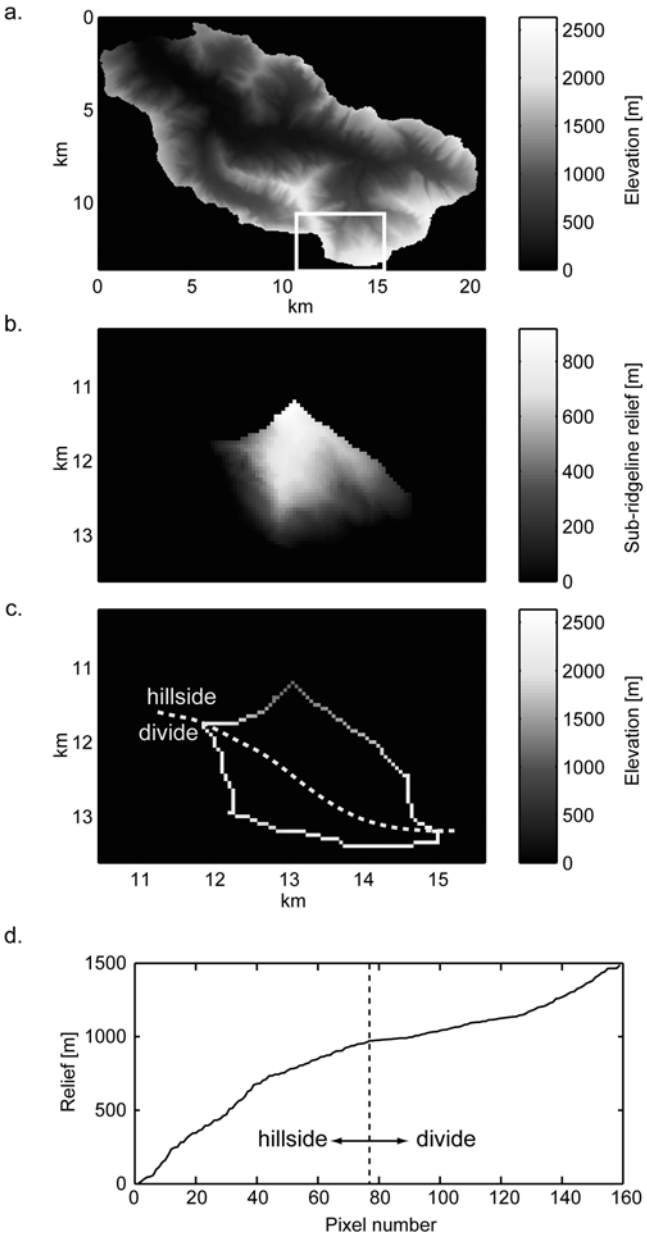

Figure 6. Illustration of hillslope relief calculation methods for the Mahitaki basin. (a) Topography of the basin. White box indicates area shown in Figures 6b and 6c, surrounding the highest point in the drainage basin. (b) Sub-ridgeline relief for the subset of the drainage basin draining through the point on the cirque floor below the highest point in the basin. (c) Elevations around the edge of the subbasin in Figure 6b, indicating points on the drainage divide of the Mahitaki basin versus points on the hillside. (d) Ranked relief values (elevations minus elevation of the subbasin outlet) for the edge (rim) of the subbasin. An inflexion separates points located on the drainage divide from those on the hillside.

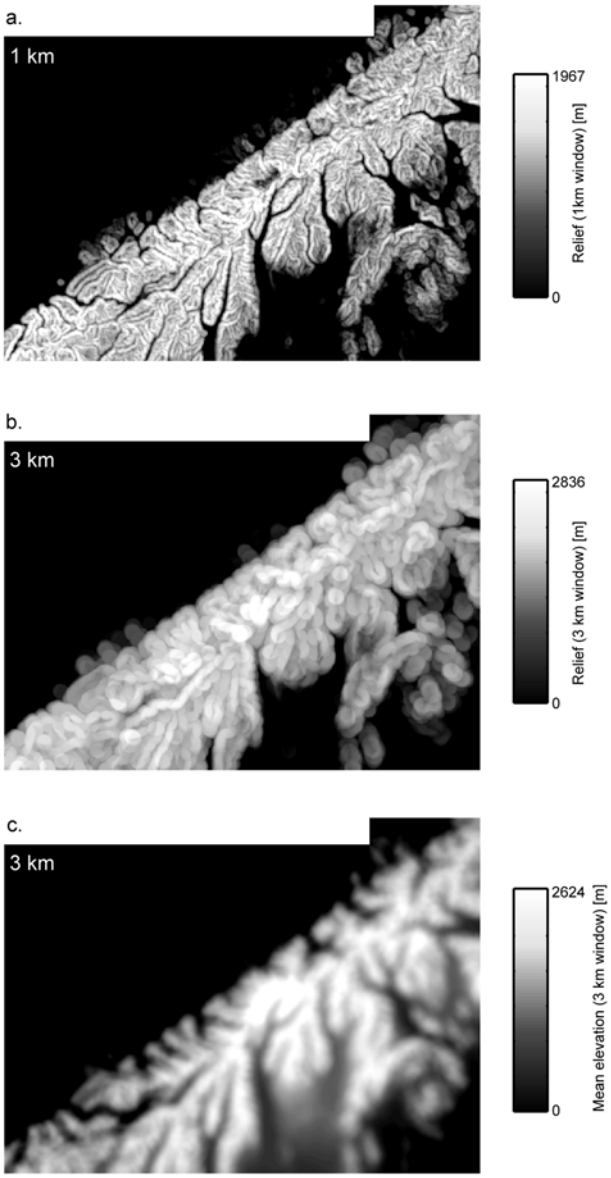

Figure 7. (a) Relief (maximum minus minimum elevation) in the Southern Alps for a 1 km radius moving circular window, calculated from the 50 m digital elevation model (DEM). (b) Relief for a 3 km radius moving circular window. (c) Mean elevations within a 3 km radius moving circular window.

have modest changes in elevation along their length, whereas the descent down the hillside to the cirque reflects steeper topography. If the relief values are sorted and plotted, there is a clear break between points on the ridgeline and on the hillside (Figure 6d). We isolated the ridgeline points, and calculated their mean and standard deviation.

5. Results

5.1. Relief and Mean Elevation

[27] Our moving window maps are shown in Figure 7. The relief maps highlight the length scale of relief in the Southern Alps. Noting the different maximum values on the shading ramp, at a 1 km radius (Figure 7a), the map tends to pick out the relief on individual hillslopes and in individual drainage basins, whereas at a 3 km radius (Figure 7b), almost the entire relief of the range is covered, highlighting a broader region of higher relief in the center of the study area, where rock uplift rates are most rapid (Figure 1). The 3 km radius mean elevation map (Figure 7c) shows regional variations in mean elevations, and concurs with the interpretation of the swath profile (Figure 1) that mean elevations correlate with rock uplift rate rather than ELA in the Southern Alps. Maximum elevations (Aoraki/Mt Cook region) are also associated with the most rapid rock uplift rates. This contradicts a literal interpretation of the glacial buzzsaw hypothesis.

[28] We present both S-N and W-E swath profiles through the Nanga Parbat massif (Figure 4). High peaks, such as Nanga Parbat itself, are clearly highlighted in the maximum elevations, but despite spectacular peaks and deep gorges, mean elevations vary surprisingly little here, except in the Kashmir Valley to the south of Nanga Parbat. On the W-E profile, mean elevations at the western end are reduced because the profile runs along the Indus. On the whole, then, the evidence here tends to favor the glacial buzzsaw hypothesis. The glaciated landscapes of the Nanga Parbat region and the Southern Alps apparently respond differently to spatial variations in rock uplift rate.

5.2. Hypsometry

[29] Figure 5 shows representative examples of hypsometry. The Callery River, just north of Aoraki/Mt Cook, experiences faster rock uplift than the Kokatahi River, near the northern end of the study transect (see Figures 1 and 2). The higher rock uplift rate causes a shallower slope in the cumulative frequency plot (equivalent to a wider elevation range in the basic hypsometry plot, Figure 5a), and suggests that glacial landscapes overall steepen in response to faster rock uplift rates, in a fashion broadly similar to their fluvial counterparts. However, in general we reproduce the major result of *Brozovic et al.* [1997], a close correlation between the ELA and the dominant peak in the frequency distribution of elevations. Given the reduced relief in the Southern Alps compared with the Nanga Parbat region, the peak in the frequency distribution of elevations is less dramatic. The Patro and Ameges basins face one another across the Indus River, but the Patro lies within the rapid rock uplift zone of the Nanga Parbat massif, draining from the west side of the mountain, whereas the Ameges lies in the slower rock uplift zone to the west. The pattern seen in the hypsometry and cumulative frequency plots (Figures 5c and 5d) is much the same as that for the Southern Alps examples described above, except that the uppermost two per cent or so of the Patro lies across a range of almost 1500m (Figure 5d), far greater than the equivalent $\sim$500m for the Callery.

5.3. Longitudinal Profiles

[30] Other than foot-of-headwall elevations (see section 5.4), we do not see any systematic changes in valley floor elevations for the glacially dominated sections of longitudinal profiles (Figure 3) in relation to rock uplift rate in either the Southern Alps or the Nanga Parbat region. Steepness values highlight the low gradient of this glacially

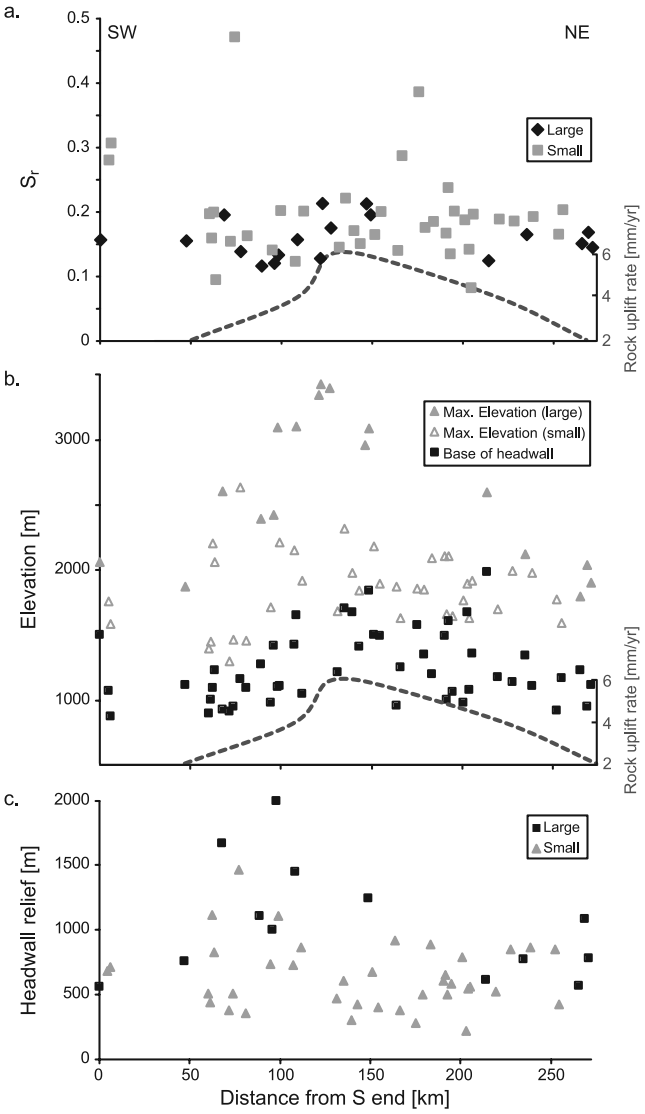

Figure 8. Sections along the Southern Alps. (a) S_r values for the glaciated portions (segment 2 in Figure 3) of all of the basins in this study. Black symbols highlight the larger basins (A > 30 km^2) that reach back to the range crest, and gray symbols are smaller basins (A < 30 km^2) that do not reach the range crest. Dashed curve indicates uplift rate pattern [*Tippett and Kamp*, 1993]. Notice the slight increase in S_r values for the large basins in the more rapidly uplifting, central portion of the study range. (b) Base-of-headwall heights and maximum elevations. Basins with ice caps excluded. Dashed curve indicates rock uplift rate pattern [*Tippett and Kamp*, 1993]. Squares indicate base-of-headwall elevation beneath the highest point on the rim of the basin. Open (small basins <30 km^2, not reaching the range crest) and solid (large basins, >30 km^2, reaching the range crest) triangles indicate maximum elevation within each basin. The headwall relief is the interval between the base of the headwall and the highest point on the basin rim. Base-of-headwall elevation rises slightly in the rapidly uplifting zone (slight steepening of the valley floor), while the highest points are significantly higher here. Thus the headwalls are taller in the rapidly uplifting zone. (c) Distribution of headwall relief in the Southern Alps.

dominated section. Given the different ranges of drainage basin areas in our two study sites, for the Southern Alps we employed a reference area, A_r, of 5×10^6 m^2, while for the Nanga Parbat region a reference area of 10^7 m^2 was used. The value of A_r chosen does not affect the pattern of the results. Figure 8a and Table 1 show S_r values for each of the basins in our Southern Alps transect. We have distinguished the larger basins (drainage area greater than 30 km^2) that developed significant glaciers and extend from the range front to the range crest from the smaller basins that do not reach the range crest. The larger basins around Aoraki/Mt Cook are slightly steeper than those to the north and south. Some of the smaller basins follow this pattern, but there is wide scatter in their steepness. The elevations of the bases of the hillslopes (Figure 8b) show a similar pattern, they rise slightly in association with more rapid rock uplift. Otherwise, valley floors are not noticeably higher in elevation in the region of rapid rock uplift than they are elsewhere.

[31] Figure 9 and Table 2 show S_r values for a selection of basins in the Nanga Parbat region. The larger basins (drainage area greater than 100 km^2) have shallow reference slopes even in the rapid rock uplift zone, but the smaller basins have higher S_r values either within, or closely adjacent to, the rapid rock uplift zone of the Nanga Parbat-Haramosh axis. Again, longitudinal profiles do not suggest any systematic variations in the elevations of valley floors in association with spatial variations in rock uplift rate.

[32] In summary, our results suggest that smaller, glaciated basins steepen somewhat in response to more rapid rock uplift. As the glaciers increase in size, however, toward the largest cases in the Nanga Parbat region, the tendency to steepen decreases; glaciated valleys can have remarkably gentle downvalley gradients even in zones of very rapid rock uplift.

5.4. Hillslope Relief

[33] Our three different measures of hillslope relief in the Southern Alps are strongly correlated (Figure 10), so in the discussion that follows we focus on the "headwall relief", the height above the cirque floor of the highest point within the drainage basin. Subridgeline relief and rim relief follow the same spatial trends along the Southern Alps. The relationship between headwall relief and rock uplift rate is shown in Figure 8c (see also Table 1). Although there is some scatter, the foot of hillslope elevations (Figure 8b) are on average ~500 m higher in the central portion of the study area (reflecting minor steepening of glaciated sections), but there is a far more striking rise in hillslope heights/relief. The correlation across each of our relief measures indicates that these are not tall hillslopes on the sides of a few isolated horns; the cirques are indeed more deeply incised into the topography as a whole where rock uplift is more rapid.

[34] In the Nanga Parbat region the development of tall headwalls is even clearer (Figure 11 and Table 2). Here hillslopes can exceed 3 km, a height that can represent around half of the basin relief and approaches half of the height of the peaks above sea level. All of the >2 km hillslopes lie within the zone of rapid rock uplift, or close to it. There are similar tall hillslopes in other parts of the Himalaya, such as the Manaslu region of Nepal [*Whipple*

Table 1. Data From the Southern Alps[a]

Basin Name	Drainage Area, km^2	S_r	Headwall Slope, degrees	Headwall Relief, m
Styx	54.4	0.14	31.5	783
Kokatahi	95.6	0.17	28.1	1084
Toaroha	62.1	0.15	18.2	568
Muriel	7.3	0.20	27.8	423
Diedrich	9.6	0.17	27.2	851
Dickson	16.2	0.19	33.5	866
Tuke	36.9	0.16	24.2	777
Kakapotahi	26.4	0.19	26.0	854
MacGregor	11.3	0.19	33.0	524
Waitaha	121	0.12	43.3	614
Hendes	15.4	0.20	29.1	565
Amethyst	15.9	0.08	29.5	546
Hot Spring	22.1	0.14	25.8	221
Tribute	10.5	0.19	30.3	787
Dry	5.1	0.20	32.3	581
Wilberg	20.8	0.13	26.1	502
Rata	3.8	0.24	37.3	655
North McCulloughs	17.8	0.17	32.9	611
Littleman	13.4	0.18	33.3	892
Mcculloughs	7.4	0.18	34.5	501
Dale	19.4	0.39	26.1	282
Gaunt	8.3	0.29	36.2	377
Darnley	15.9	0.14	32.6	918
Potters	9.5	0.20	34.9	404
Tartare	27.6	0.16	32.0	673
Callery	94.6	0.20	42.2	1243
Waiho	65.7	0.21	32.0	399
Docherty	10.5	0.15	41.0	426
Omoeroa	10.7	0.17	28.2	306
Waikukupa	22.4	0.22	19.4	607
Clearwater	3.6	0.14	31.6	467
Fox	87.9	0.17	43.9	737
Balfour	36.2	0.21	57.2	358
Cook	74.3	0.13	39.3	795
Havelock	10.5	0.20	35.4	862
Copland	112	0.16	41.8	1451
Architect	24.0	0.12	37.6	726
Regina	17.7	0.20	34.2	1107
Douglas	69.8	0.13	28.3	1993
Karangarua	47.0	0.12	51.2	999
Manakaiaua	10.3	0.14	36.1	738
Makawhio	105	0.12	36.4	1110
Flagstaff	10.8	0.16	34.8	359
Mahitaki	144	0.14	27.4	1466
Doughboy	3.3	0.47	27.5	509
Blackwater	3.1	0.15	35.7	383
Otoko	83.6	0.19	22.7	1671
Darkness	12.5	0.09	37.4	829
Tunnel	13.5	0.20	35.4	1114
Stew	10.2	0.16	26.3	444
Panel	3.1	0.20	25.0	506
Moeraki	58.1	0.15	45.5	756
Eggerling	3.5	0.31	29.0	711
Warren	5.2	0.28	37.0	686
Turnbull	147	0.16	29.3	558

[a]Basins listed from north to south. Large basins exceed 30 km^2.

and Brocklehurst, 2000], and a similar correlation between hillslope height and rock uplift rate in southern Alaska [*Meigs and Sauber*, 2000; *Merrand and Hallet*, 2000].

6. Discussion

6.1. Summary of Observations

[35] Our mean elevation and relief maps and swath profile of the Southern Alps indicate that both mean elevations and relief are higher toward the center of our study area, around Aoraki/Mt Cook, where rock uplift rates are highest. However, swath profiles along and across the Nanga Parbat–Haramosh massif indicate mean elevation does not vary, whereas relief does, in relation to rock uplift rate. The observation from our longitudinal profiles that valley floor elevations do not vary in association with spatial changes in rock uplift rate suggests that glaciers are capable of eroding valley floors at rates comparable to the most rapid rock uplift rates. Furthermore, if the glaciers are sufficiently large, they can do so while maintaining a shallow downvalley gradient. In the larger basins (>30 km^2) of the Southern Alps that develop substantial glaciers, we observe only minor, if any, steepening of the longitudinal profile in association with greater rock uplift rates. In the Nanga Parbat region, the largest glaciated basins (drainage areas of 100 km^2), retain shallow downvalley gradients even where rock uplift is most rapid, while smaller basins are steeper in the rapid rock uplift zone than in the neighboring regions. Thus glacier size seems to represent a determining factor in the glacier's response to rock uplift.

6.2. Landscape Response to Climate Change

[36] Figure 12 summarizes, in cartoon form, the main features of glacial valley longitudinal profiles that we have observed in settings with slow [*Brocklehurst and Whipple*, 2002, 2006] and rapid (this study) rock uplift. In the smaller, glaciated basins of the Sierra Nevada (Figure 12a), glaciers lower valley floors and ridgelines above the mean Quaternary ELA. Below this the valleys are widened to a U-shaped cross section, but the longitudinal profile does not deviate significantly from a typical fluvial profile. Larger, glaciated basins (Figure 12b) show glacial steps down to much lower elevations. In tectonically more active locations, smaller glaciers apparently steepen in response to rapid rock uplift (Figure 12c), although less so than one would expect for a fluvial setting. For example, *Kobor and Roering* [2004], found a more than fourfold variation in channel steepness values amongst the fluvial channels of the Oregon Coast Range. Although rock uplift rate data are sparse in the Oregon Coast Range, this appeared to correspond directly with a fourfold variation in rock uplift rate. For the Southern Alps and the Nanga Parbat region, there are threefold and two- to five-fold variations in rock uplift rate, respectively, but in each case downvalley steepness varies at most by a factor of two in the smaller drainage basins. Meanwhile, the larger glaciers (Figure 12d) can apparently incise at rates comparable to the most rapid rock uplift without any steepening of the longitudinal profile.

[37] The contrasting erosional behavior as a function of glacier size probably reflects a relationship between ice flux and erosion rate. The *Hallet et al.* [1996] compilation of glacial erosion rates demonstrated a link between glacier size and mean erosion rate, while *Anderson et al.* [2006] showed that the major features of glacial longitudinal profiles can be explained with a simple model where erosion rate is proportional to ice discharge per unit valley width. The link between ice flux and erosion rate is also envisaged by theoretical formulations for glacial erosion [e.g., *Hallet*, 1979; *Hallet*, 1996]. A secondary effect is the longevity of glaciers of different sizes; larger glaciers formed in larger drainage basins will tend to have a larger accumulation area and hence be longer lived. The smaller

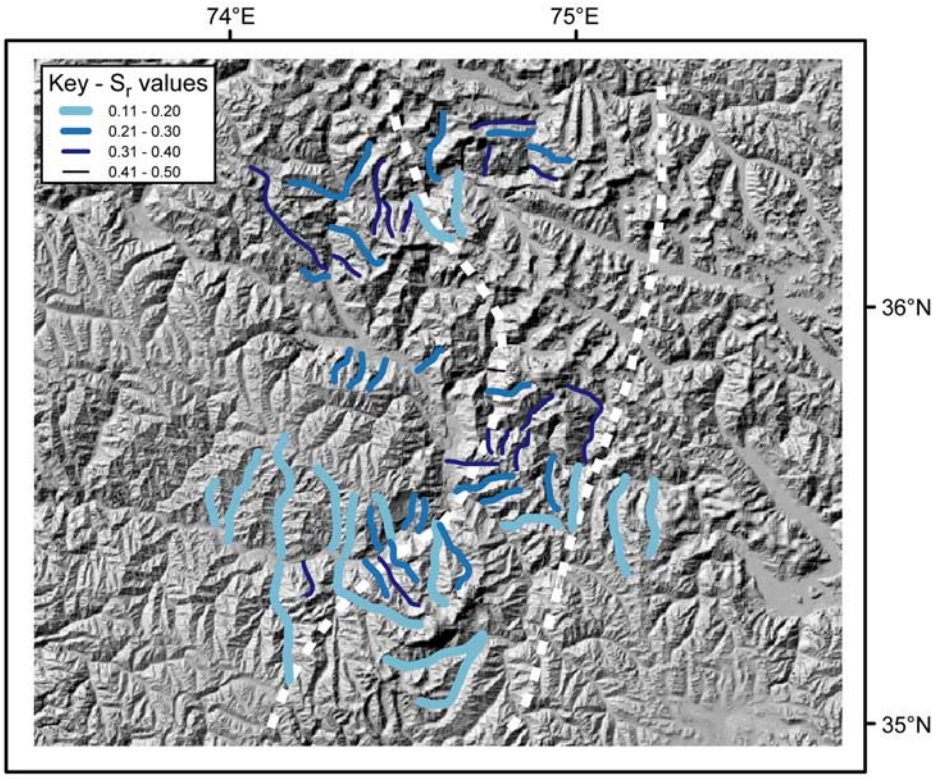

Figure 9. Distribution of S_r values for glacially dominated portions of longitudinal profiles for basins in the study area around Nanga Parbat, values as indicated in the key. Variations in S_r values are subtle. However, the steepest basins (highest S_r) lie within or adjacent to the rapid rock uplift zone, bounded by white dashed curves. The largest basins ($A > 100$ km^2) within this zone have lower reference slope values, indistinguishable from basins outside this zone.

basins in the Southern Alps that show scattered steepness values might not have experienced sustained glacial erosion. In addition, interglacial fluvial conditions may have a greater influence on the longitudinal profiles of smaller drainage basins less persistently occupied by ice, which may further contribute to their greater sensitivity to rock uplift rate. *Merrand and Hallet* [2000] suggested that rapid incision by large glaciers might be achieved by high basal water pressures (approaching 80% of the hydrostatic pressure). This would allow the glacier to be close to floating, facilitating extremely efficient erosion by plucking/quarrying. However, the details of subglacial hydrology in relation to glacier size, dynamics and erosion remain an outstanding question.

[38] The enormous scale of the cirque headwall indicates that it has not eroded at the same rate as valley incision at some point in its development. The discrepancy in erosion rates may continue. Direct measurements of headwall retreat and glacial valley incision rates in alpine settings are sparse, in particular headwall retreat rates in a directly comparable setting. *Heimsath and McGlynn* [2007] determined a headwall retreat rate of 0.77 mm/yr for a glaciated basin on the north slope of the Annapurna Range. *Brook et al.* [2006] and *Matsuoka and Sakai* [1999] calculated mean headwall retreat rates of 0.44 mm/yr and 0.1 mm/yr in the Ben Ohau Range, New Zealand, and Japanese Alps, respectively. *Gardner and Jones* [1993] determined an incision rate of 4–6 mm/yr for the Raikot Glacier on the northern flank of Nanga Parbat. If our interpretation that glacial incision rates must be broadly comparable to the extremely rapid exhumation rates at Nanga Parbat is correct, this suggests glacial incision rates of ~2–10 mm/yr. It would appear that valley incision may outpace headwall erosion.

[39] The development of tall cirque headwalls may reflect the presence of a threshold glacier size for efficient erosion and undermining of the headwall; small cirque glaciers are unable to keep pace with rapid rock uplift, and through time cirque floor is replaced with hillslopes, accompanied by a dramatic change in gradient and relief. There might be an effect local to the base of the headwall, that it is just here that erosion is inefficient; perhaps these environments are too dry to support efficient erosion in the region of the bergschrund. Slower hillslope erosion processes in this permanently frozen, arid setting will also aid the headwall to grow to staggering heights. The effectiveness of coupling between cirque glacier erosion and headwall erosion is an outstanding question.

[40] Late Cenozoic climate change and the spread of alpine glaciation may have significantly reshaped many tectonically active mountain ranges. Fluvial and glacial erosion respond differently to climate change. Glaciers can reduce valley gradients, while hillslopes lengthen and drainage density decreases. Glaciers may well erode most efficiently as a consequence of a cycle of advance and retreat, allowing weathering of destabilized valley sidewalls (as opposed to higher-elevation cirque headwalls which

Table 2. Data From the Nanga Parbat Region[a]

Basin Number	Uplift Rate	Location	Drainage Area, km^2	S_r	Headwall Slope, degrees	Headwall Relief, m
1	medium	W	25.6	0.25	30.0	1158
2	medium	W	72.4	0.17	25.8	545
3	medium	W	274	0.15	44.1	1639
4	high		79.4	0.35	30.7	563
5	low	W	59.7	0.20	22.5	650
6	medium	W	40.1	0.27	27.9	1552
7	high		48.0	0.32	34.6	673
8	medium/high	W	45.1	0.32	28.5	1676
9	low	E	32.2	0.19	24.0	909
10	medium	W	43.5	0.31	39.9	1160
11	high		198	0.14	39.5	1462
12	medium	W	106	0.23	41.3	1918
13	medium	W	36.5	0.19	34.0	392
14	medium/high	W	231	0.19	36.0	3582
15	high		98.2	0.19	39.8	1651
16	medium	W	33.8	0.21	48.2	1258
17	low	W	113	0.22	21.2	1238
18	medium	W	119	0.22	38.0	2605
19	medium	W	58.8	0.31	28.7	1628
20	medium/high	E	74.7	0.20	29.8	1131
21	medium	W	35.0	0.34	27.6	1726
22	medium	W	44.0	0.29	34.6	1583
23	low	W	226	0.17	23.2	713
24	low	W	45.1	0.17	34.9	467
25	high		23.1	0.45	33.0	2166
26	high		64.5	0.18	34.0	552
27	high		59.9	0.29	29.4	2761
28	high		137	0.20	45.0	1672
29	medium/high	W	48.0	0.23	26.2	301
30	high		28.3	0.46	32.8	2651
31	medium	W	45.2	0.28	30.4	257
32	high		40.7	0.24	38.5	457
33	medium/low	W	151	0.14	28.2	181
34	high		23.0	0.36	32.1	2059
35	medium	W	35.8	0.28	53.8	219
36	medium/low	W	42.5	0.21	28.8	804
37	high		20.6	0.39	35.4	1515
38	high		63.1	0.12	54.5	1358
39	high		32.6	0.36	38.4	2205
40	high		54.7	0.26	41.1	1066
41	medium	W	44.2	0.11	32.5	745
42	medium/high	W	78.0	0.31	42.7	1412
43	high		356	0.27	44.7	2953
44	high		29.5	0.48	41.9	1984
45	high		38.8	0.39	45.2	1967
46	high		66.1	0.25	32.5	347
47	high		331	0.13	42.5	3111
48	high		50.7	0.36	46.2	1335
49	medium	**W**	36.8	0.27	26.9	1171
50	high		55.5	0.25	26.7	1155
51	medium	W	40.8	0.24	26.5	1321
52	high		90.1	0.26	36.7	1485
53	high		27.0	0.27	42.2	1910
54	medium/low	W	517	0.14	21.7	1895
55	medium	E	88.8	0.18	24.5	1217
56	medium/high	E	355	0.21	51.0	1864
57	medium/high	E	22.5	0.37	43.9	1981
58	high	E	104	0.17	43.6	1799
59	medium	E	20.7	0.36	37.0	2247

[a]Uplift rates: high signifies rapid rock uplift in the Nanga Parbat-Haramosh massif (NPMH), medium rates of rock uplift lie to either side, and low rates lie further outboard of the NPHM. Locations to west or east of NPHM. Large basins exceed 100 km^2. Diamir Basin is Basin 14, Ameges is 2, and Patro is 42.

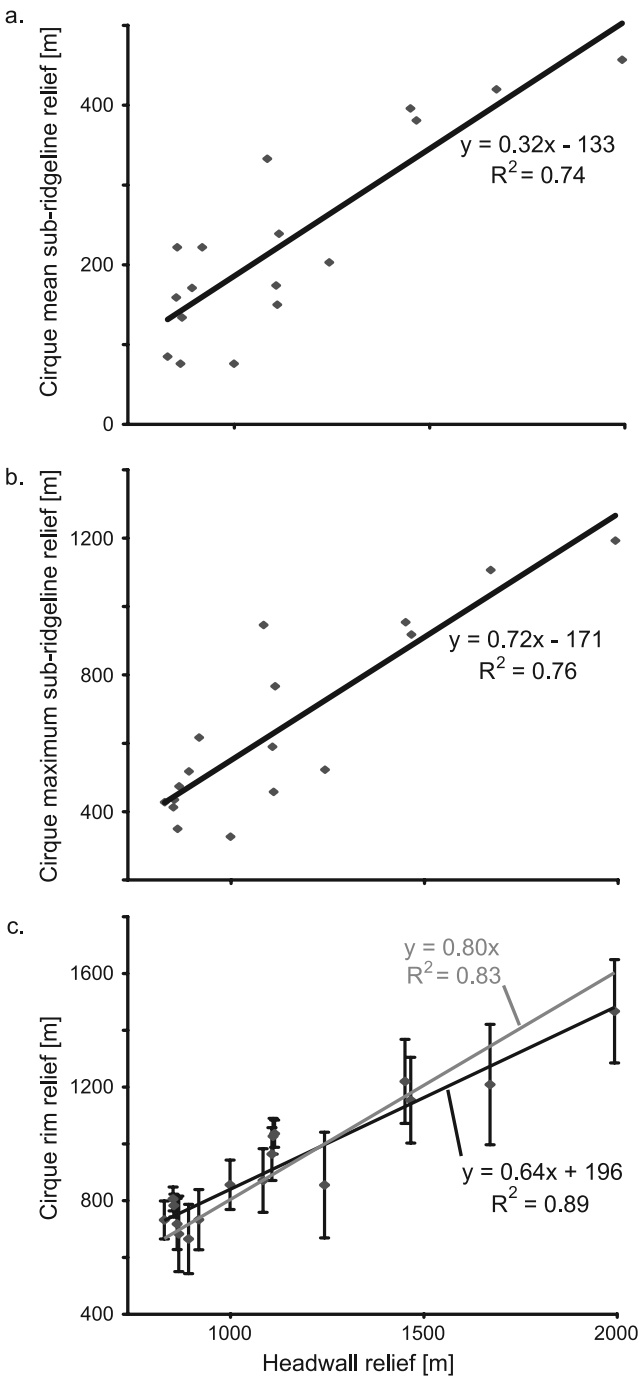

Figure 10. Comparison of results using different hillslope relief methods (see text for definitions). (a) Mean subridgeline relief (for all points within subsection of cirque) versus headwall relief, along with best-fit linear least squares regression. (b) Maximum subridgeline relief within subsection of cirque versus headwall relief, along with best-fit linear least squares regression. (c) Mean values of rim relief, plus or minus standard deviation, versus maximum headwall relief, along with best-fit linear least squares regression (black curve) and linear least squares regression forced to have an intercept of 0 (gray curve).

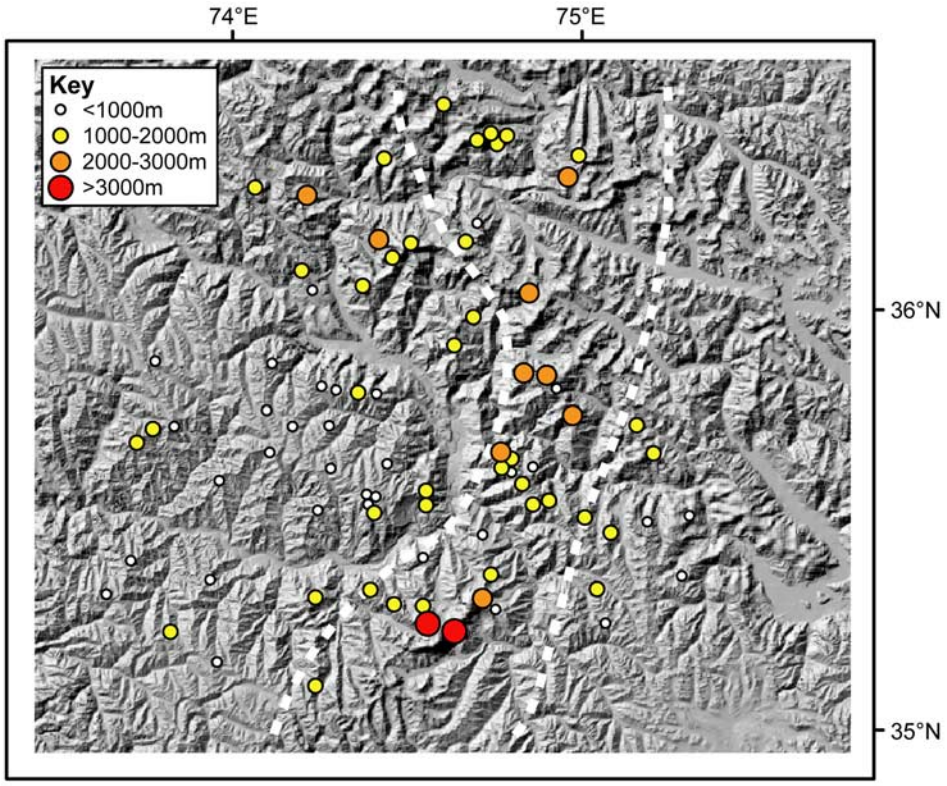

Figure 11. Distribution of headwall heights around Nanga Parbat, heights as indicated in the key. Notice that all of the tallest headwalls are focused in or adjacent to the high uplift zone, bounded by white dashed curves.

may be resistant to weathering because of extreme cold and aridity) during glacier retreat stages, and efficient removal of colluvial debris during glacier advance. Rivers are a more constant presence in the landscape, although their ability to erode depends on storminess of the climate, sediment load, and other climate-related parameters [e.g., *Snyder et al.*, 2003; *Whipple*, 2004; *Whipple et al.*, 1999].

6.3. Glacial Buzzsaw Hypothesis

[41] The shallow downvalley gradients of large glaciers support the glacial buzzsaw hypothesis [*Brozovic et al.*, 1997]. However, formation of tall hillslopes steepens the landscape as a whole, as observed in the cumulative frequency hypsometry, requiring modification of the glacial buzzsaw hypothesis. In the Nanga Parbat case, swath profiles confirm the original observations of *Brozovic et al.* [1997], that mean elevations are almost uniform across the massif. Here, the areally extensive large glaciers dominate, perhaps because the zone of rapid rock uplift in the Nanga Parbat massif is localized because of structural control, creating a narrow zone with dramatic headwalls. Mean topography rises more significantly in association with rapid rock uplift in the Southern Alps. This may reflect the broader region of rapid rock uplift, where a wider zone of tall hillslopes constitutes a sufficiently high percentage of the landscape to raise regional mean elevations.

6.4. Hillslopes in Glaciated Landscapes

[42] The major response of glaciated landscapes to rapid rock uplift occurs in the hillslopes surrounding these alpine basins [*Anderson*, 2005]. From this study we cannot directly infer if these hillslopes are continuing to lengthen. These headwalls can comprise between a third and a half of the peak height above sea level, and clearly represent an

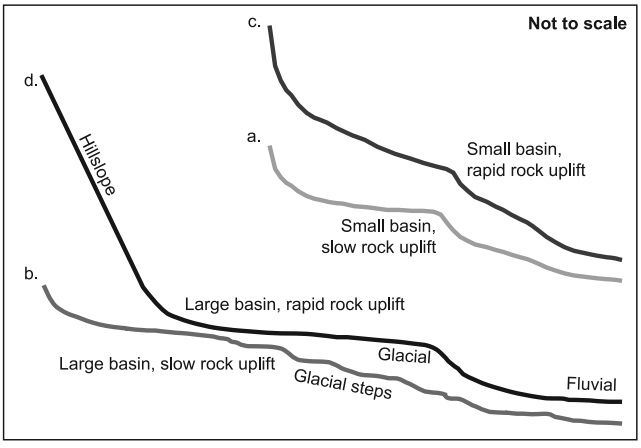

Figure 12. Cartoon sketch illustrating the key differences between glacial valley longitudinal profiles in different settings: (a) small, glaciated basin in a slowly uplifting range (e.g., Independence/Lone Pine Creek, eastern Sierra Nevada); (b) large, glaciated basin in a slowly uplifting range (e.g., Big Pine/Bishop Creek, eastern Sierra Nevada); (c) small, glaciated basin in a rapidly uplifting range (e.g., Patro Basin, Nanga Parbat region); (d) large, glaciated basin in a rapidly uplifting range (e.g., Diamir Basin, Nanga Parbat region).

increase in relief. The observation that mean elevation is not strictly controlled by a glacial "buzzsaw", though minor when compared to fluvial steepening of a landscape, may have important consequences. In a tectonically active mountain belt, while mean topography may decline as a result of the onset of glacial erosion, peak heights may indeed rise [*Molnar and England*, 1990]. Some examples of the possible influences of steep, ice-free, bedrock hillslopes, especially when they reach several kilometers tall, follow.

[43] Giant hillslopes are sources of snow accumulation and redistribution [e.g., *Hewitt*, 1993]. Snow does not accumulate on the steepest slopes; it avalanches to the floor below. These avalanches can be a major contributor to glacier mass balance [e.g., *Gardner and Jones*, 1993; *Harper and Humphrey*, 2003; *Phillips et al.*, 2000]. High ridgelines also shade the valley floor, again affecting mass balance. Avalanches and rockslides are major agents of debris transfer to the glaciers below [e.g., *Arsenault and Meigs*, 2005; *Hewitt*, 1993, 1998]. Giant hillslopes form a major component of peak elevation. These peaks, though spatially rare, can be responsible for disrupting local atmospheric circulation patterns, and determining the effects of orographic precipitation, and the wind-blown redistribution of snow [*Brocklehurst and MacGregor*, 2005].

[44] We suggest that hillslopes of this length may represent a useful geomorphological tool for identifying zones of rapid rock uplift within a glaciated mountain range, while acknowledging the potentially complicating influence of variations in rock strength [e.g., *Augustinus*, 1992, 1995]. Following this approach, we would suggest that the zone of rapid rock uplift shown on Figure 2 may extend further to the west, around Rakaposhi, since it is in this region that the only giant hillslopes outside of the mapped rapid rock uplift zone occur. However, this idea needs further testing before we can confidently employ the presence of tall cirque headwalls as an indicator of rapid rock uplift.

6.5. Implications for Glacial Erosion in Landscape Evolution Models

[45] In addition to interesting feedback relationships in existing tectonic glacial landscape evolution models [*Merrand and Hallet*, 2000; *Tomkin*, 2003, 2007], there are three important considerations that motivate the incorporation of glacial erosion processes in geodynamic models: (1) the damped response of mean topography to rock uplift in glacially versus fluvially controlled landscapes; (2) the contrasting development of relief in fluvial and glacial landscapes, since this will determine the flexural isostatic response to incision, set peak heights, and control local atmospheric dynamics and glacier mass balance; and (3) the different responses of the fluvial and glacial systems to climate change.

[46] In the case of low rock uplift rates, glacial erosion develops low valley gradients that lower mean topography [*Brocklehurst and Whipple*, 2002, 2006]. In the face of more rapid rock uplift, glaciated landscapes steepen little, if at all, while their fluvial counterparts steepen significantly. These represent very different upper boundary conditions to a geodynamic model. In denuding the landscape in a noticeably different fashion from fluvial erosion, glaciers may well influence orogen development. Although not directly comparable, *Beaumont et al.* [1996] illustrate significant differences in the internal dynamics of their model of the Southern Alps between experiments in which surface denudation is total (topography is instantly eroded to sea level) and those in which surface denudation is more modest. Developing this theme, *Tomkin* [2007] used a tectonic glacial landscape evolution model to demonstrate that both the style and spatial extent of glacial erosion affect the topography and tectonic response to erosion in an active orogen.

7. Conclusion

[47] We have carried out a series of topographic analyses to elucidate the response of glaciated landscapes to spatial variations in rock uplift rate, emphasizing some of the most extreme rock uplift rates in the world. The principle response of glaciated landscapes to rapid rock uplift is the development of towering hillslopes, comprising between a third and a half of the elevation of some of the world's highest peaks. This cirque headwall lengthening and (downvalley) advance is commensurate with a decrease in drainage density. The lengthening of hillslopes causes mean elevation to rise slightly with increasing rock uplift rate, although less than expected in nonglaciated ranges. A secondary response is a minor steepening of the section of the valley floor dominated by glaciers, although the largest glaciated valleys (>100 km^2 for Nanga Parbat, >30 km^2 for the Southern Alps) are strikingly unaffected in this regard. Thus the size of a glacier seems to affect its response to rapid rock uplift. Furthermore, there is an apparent threshold cirque glacier size below which glacial erosion cannot keep pace with rapid rock uplift. Replacement of valley floor by steep hillslope allows headwalls to grow and causes drainage density to decrease.

[48] Peak heights in glaciated mountain belts could play a crucial role in the relationship between climate change and tectonic processes, while periglacial hillslopes have important implications for glacier mass balance and debris transfer to glacier surfaces. Thus the controls on the development of hillslopes in tectonically active, glaciated mountain belts represent an important area for future research. Our results highlight important distinctions between the evolution of fluvial and glacial landscapes, which have significant consequences for the interplay between surface and geodynamic processes, and motivate the further development of landscape evolution models and coupled tectonic erosion models incorporating glacial erosion.

[49] **Acknowledgments.** This work was supported by NSF grant EAR-9980465 (to K.X.W.), NASA grant SENH99-0209-0172 (to K.X.W.), a NASA Earth System Science Graduate Fellowship (to S.H.B.), and a CIRES Visiting Fellowship (to S.H.B.). We would like to thank Bob Anderson, Bernard Hallet, Doug Burbank, and Chris Beaumont for valuable discussions, Bob Anderson, Ben Crosby, Mike Ellis, Emma Finch, David Mohrig, Mike Oskin, and Jon Tomkin for considered comments on earlier versions of this manuscript, and Mike Oskin and Kelly MacGregor for thorough, constructive reviews.

References

Adams, J. (1980), Contemporary uplift and erosion of the Southern Alps, New Zealand, *Geol. Soc. Am. Bull.*, *91*, 1–114.

Anderson, R. S. (2005), Teflon peaks: The evolution of high local relief in glaciated mountain ranges, *EOS Trans. AGU*, *86*(52), Fall Meet. Suppl., Abstract H33F-04.

Anderson, R. S., P. Molnar, and M. A. Kessler (2006), Features of glacial valley profiles simply explained, *J. Geophys. Res.*, *111*, F01004, doi:10.1029/2005JF000344.

Arsenault, A. M., and A. J. Meigs (2005), Contribution of deep-seated bedrock landslides to erosion of a glaciated basin in southern Alaska, *Earth Surf. Processes Landforms*, *30*, 1111–1125.

Augustinus, P. C. (1992), The influence of rock mass strength on glacial valley cross-profile morphometry: A case study from the Southern Alps, New Zealand, *Earth Surf. Processes Landforms*, *17*, 39–51.

Augustinus, P. C. (1995), Glacial valley cross-profile development: The influence of in-situ rock stress and rock mass strength, with examples from the Southern Alps, New Zealand, *Geomorphology*, *14*, 87–97.

Batt, G. E., and J. Braun (1999), The tectonic evolution of the Southern Alps, New Zealand: Insights from fully thermally coupled dynamical modelling, *Geophys. J. Int.*, *136*(2), 403–420.

Batt, G. E., J. Braun, B. P. Kohn, and I. McDougall (2000), Thermochronological analysis of the dynamics of the Southern Alps, New Zealand, *Geol. Soc. Am. Bull.*, *112*(2), 250–266.

Beaumont, C., P. Fullsack, and J. Hamilton (1992), Erosional control of active compressional orogens, in *Thrust Tectonics*, edited by K. R. McClay, pp.1–18, Chapman and Hall, London.

Beaumont, C., P. J. J. Kamp, J. Hamilton, and P. Fullsack (1996), The continental collision zone, South Island, New Zealand: Comparison of geodynamical models and observations, *J. Geophys. Res.*, *101*(B2), 3333–3359.

Beaumont, C., R. A. Jamieson, M. H. Nguyen, and B. Lee (2001), Himalayan tectonics explained by extrusion of a low-viscosity crustal channel coupled to focused surface denudation, *Nature*, *414*, 738–742.

Benn, D. I., and D. J. A. Evans (1998), *Glaciers and Glaciation*, 734 pp., Arnold, London.

Bookhagen, B., D. Fleitmann, K. Nishiizumi, M. R. Strecker, and R. C. Thiede (2006), Holocene monsoonal dynamics and fluvial terrace formation in the northwest Himalaya, India, *Geology*, *34*(7), 601–604.

Bookhagen, B., R. C. Thiede, and M. R. Strecker (2005), Late Quaternary intensified monsoon phases control landscape evolution in the northwest Himalaya, *Geology*, *33*(2), 149–152.

Braun, J., D. Zwartz, and J. H. Tomkin (1999), A new surface-processes model combining glacial and fluvial erosion, *Ann. Glaciol.*, *28*, 282–290.

Brocklehurst, S. H. (2002), Evolution of topography in glaciated mountain ranges, Ph.D. thesis, Mass. Inst. of Technol., Cambridge.

Brocklehurst, S. H., and K. R. MacGregor (2005), The role of wind in the evolution of glaciated mountain ranges: Field observations and insights from numerical modelling, *EOS Trans. AGU*, *86*(52), Fall Meet. Suppl., Abstract H51C-0390.

Brocklehurst, S. H., and K. X. Whipple (2002), Glacial erosion and relief production in the eastern Sierra Nevada, California, *Geomorphology*, *42*(1–2), 1–24.

Brocklehurst, S. H., and K. X. Whipple (2004), Hypsometry of glaciated landscapes, *Earth Surf. Processes Landforms*, *29*(7), 907–926.

Brocklehurst, S. H., and K. X. Whipple (2006), Assessing the relative efficiency of fluvial and glacial erosion through fluvial landscape simulation, *Geomorphology*, *75*, 283–299.

Brook, M. S., M. P. Kirkbride, and B. W. Brock (2006), Cirque development in a steadily uplifting range: Rates of erosion and long-term morphometric change in alpine cirques in the Ben Ohau Range, New Zealand, *Earth Surf. Processes Landforms*, *31*, 1167–1175.

Brozovic, N., D. W. Burbank, and A. J. Meigs (1997), Climatic limits on landscape development in the northwestern Himalaya, *Science*, *276*, 571–574.

Burbank, D. W., J. Leland, E. Fielding, R. S. Anderson, N. Brozovic, M. R. Reid, and C. Duncan (1996), Bedrock incision, rock uplift and threshold hillslopes in the northwestern Himalayas, *Nature*, *379*, 505–510.

Craw, D., E. Nelson, and P. O. Koons (2003), Structure and topographic evolution of the Main Divide in the Landsborough-Hopkins area of the Southern Alps, New Zealand, *N. Z. J. Geol. Geophys.*, *46*, 553–562.

Densmore, A. L., M. A. Ellis, and R. S. Anderson (1998), Landsliding and the evolution of normal-fault-bounded mountains, *J. Geophys. Res.*, *103*(B7), 15,203–15,219.

England, P., and P. Molnar (1990), Surface uplift, uplift of rocks, and exhumation of rocks, *Geology*, *18*, 1173–1177.

Fielding, E., B. Isacks, M. Barazangi, and C. Duncan (1994), How flat is Tibet?, *Geology*, *22*, 163–167.

Flint, J. J. (1974), Stream gradient as a function of order, magnitude, and discharge, *Water Resour. Res.*, *10*, 969–973.

Gardner, J. S., and N. K. Jones (1993), Sediment transport and yield at the Raikot Glacier, Nanga Parbat, Punjab Himalaya, in *Himalaya to the Sea: Geology, Geomorphology and the Quaternary*, edited by J. F. Shroder Jr., pp.184–197, Routledge, London.

Hales, T. C., and J. J. Roering (2005), Climate-controlled variations in scree production, Southern Alps, New Zealand, *Geology*, *33*(9), 701–704.

Hallet, B. (1979), A theoretical model of glacial abrasion, *J. Glaciol.*, *23*(89), 39–50.

Hallet, B. (1996), Glacial quarrying: A simple theoretical model, *Ann. Glaciol.*, *22*, 1–8.

Hallet, B., L. Hunter, and J. Bogen (1996), Rates of erosion and sediment evacuation by glaciers: A review of field data and their implications, *Global Planet. Change*, *12*, 213–235.

Harbor, J. M. (1992), Numerical modeling of the development of U-shaped valleys by glacial erosion, *Geol. Soc. Am. Bull.*, *104*, 1364–1375.

Harper, J. T., and N. F. Humphrey (2003), High altitude Himalayan climate inferred from glacial ice flux, *Geophys. Res. Lett.*, *30*(14), 1764, doi:10.1029/2003GL017329.

Heimsath, A. M., and R. S. McGlynn (2007), Quantifying headwall retreat rates in the Nepal High Himalaya, *Geomorphology*, in press.

Hewitt, K. (1993), Altitudinal organization of Karakoram geomorphic processes and depositional environments, in *Himalaya to the Sea: Geology, Geomorphology and the Quaternary*, edited by J. F. Shroder Jr., pp. 159–183, Routledge, London.

Hewitt, K. (1998), Catastrophic landslides and their effects on the Upper Indus streams, Karakoram Himalaya, northern Pakistan, *Geomorphology*, *26*(1–3), 47–80.

Holmes, J. A. (1993), Present and past patterns of glaciation in the northwest Himalaya: Climatic, tectonic and topographic controls, in *Himalaya to the Sea: Geology, Geomorphology and the Quaternary*, edited by J. F. Shroder Jr., pp. 72–90, Routledge, London.

Hooke, R. L. (1991), Positive feedbacks associated with erosion of glacial cirques and overdeepenings, *Geol. Soc. Am. Bull.*, *103*, 1104–1108.

Hovius, N., C. P. Stark, and P. A. Allen (1997), Sediment flux from a mountain belt derived by landslide mapping, *Geology*, *25*(3), 231–234.

Howard, A. D. (1997), Badland morphology and evolution: Interpretation using a simulation model, *Earth Surf. Processes Landforms*, *22*, 211–227.

Howard, A. D., W. E. Dietrich, and M. A. Seidl (1994), Modeling fluvial erosion on regional to continental scales, *J. Geophys. Res.*, *99*(B7), 13,971–13,986.

Jamieson, R. A., C. Beaumont, M. H. Nguyen, and B. Lee (2002), Interaction of metamorphism, deformation and exhumation in large convergent orogens, *J. Metamorph. Geol.*, *20*, 9–24.

Kamp, P. J. J. (1997), Paleogeothermal gradient and deformation style, Pacific front of the Southern Alps orogen: Constraints from fission track thermochronology, *Tectonophysics*, *271*, 37–58.

Kirby, E., K. X. Whipple, W. Tang, and Z. Chen (2003), Distribution of active rock uplift along the eastern margin of the Tibetan Plateau: Inferences from bedrock channel longitudinal profiles, *J. Geophys. Res.*, *108*(B4), 2217, doi:10.1029/2001JB000861.

Kobor, J. S., and J. Roering (2004), Systematic variation of bedrock channel gradients in the central Oregon Coast Range: Implications for rock uplift and shallow landsliding, *Geomorphology*, *62*, 239–256.

Koons, P. O. (1995), Modeling the topographic evolution of collisional belts, *Ann. Rev. Earth Planet. Sci.*, *23*, 375–408.

Korup, O. (2006), Rock-slope failure and the river long profile, *Geology*, *34*(1), 45–48.

Lague, D., and P. Davy (2003), Constraints on the long-term colluvial erosion law by analyzing slope-area relationships at various tectonic uplift rates in the Siwalik Hills (Nepal), *J. Geophys. Res.*, *108*(B2), 2129, doi:10.1029/2002JB001893.

Little, T. A., S. Cox, J. K. Vry, and G. E. Batt (2005), Variations in exhumation level and uplift rate along the oblique-slip Alpine Fault, central Southern Alps, New Zealand, *Geol. Soc. Am. Bull.*, *117*(5/6), 707–723.

MacGregor, K. C., R. S. Anderson, S. P. Anderson, and E. D. Waddington (2000), Numerical simulations of glacial valley longitudinal profile evolution, *Geology*, *28*(11), 1031–1034.

Mason, B. (1962), Metamorphism in the Southern Alps of New Zealand, *Bull. Am. Mus. Nat. Hist.*, *123*, 217–248.

Matsuoka, N., and H. Sakai (1999), Rockfall activity from an alpine cliff during thawing periods, *Geomorphology*, *28*, 309–328.

Meigs, A., and J. Sauber (2000), Southern Alaska as an example of the long-term consequences of mountain building under the influence of glaciers, *Quat. Sci. Rev.*, *19*, 1543–1562.

Merrand, Y., and B. Hallet (2000), A physically based numerical model of orogen-scale glacial erosion: Importance of subglacial hydrology and basal stress regime, *Geol. Soc. Am. Abstr. Programs*, *32*(7), A329.

Mitchell, S. E. G., and D. R. Montgomery (2006), Influence of a glacial buzzsaw on the height and morphology of the Cascade Range in central Washington State, USA, *Quat. Res.*, *65*, 96–107.

Molnar, P., and P. England (1990), Late Cenozoic uplift of mountain ranges and global climate change: Chicken or egg?, *Nature*, *346*, 29–34.

Molnar, P., and H. Lyon-Caen (1988), Some simple physical aspects of the support, structure, and evolution of mountain belts, in *Processes in*

Continental Lithospheric Deformation, edited by S. P. Clark Jr., B. C. Burchfiel, and J. Suppe, *Spec. Pap. Geol. Soc. Am.*, 179–207.
Oguchi, T. (1997), Drainage density and relative relief in humid steep mountains with frequent slope failure, *Earth Surf. Processes Landforms*, *22*, 107–120.
Oskin, M., and D. W. Burbank (2005), Alpine landscape evolution dominated by cirque retreat, *Geology*, *33*(12), 933–936.
Owen, L. A., C. H. Scott, and E. Derbyshire (2000), The Quaternary glacial history of Nanga Parbat, *Quat. Int.*, *65/66*, 63–79.
Paterson, W. S. B. (1994), *The Physics of Glaciers*, 480 pp., Elsevier, New York.
Phillips, W. M., V. F. Sloan, J. F. Shroder Jr., P. Sharma, M. L. Clarke, and H. M. Rendell (2000), Asynchronous glaciation at Nanga Parbat, northwestern Himalaya Mountains, Pakistan, *Geology*, *28*(5), 431–434.
Porter, S. C. (1975), Equilibrium-line altitudes of Late Quaternary glaciers in the Southern Alps, New Zealand, *Quat. Res.*, *5*, 27–47.
Porter, S. C. (1989), Some geological implications of average Quaternary glacial conditions, *Quat. Res.*, *32*, 245–261.
Raymo, M. E., and W. F. Ruddiman (1992), Tectonic forcing of Late Cenozoic climate, *Nature*, *359*, 117–122.
Richards, B. W. M., D. I. Benn, L. Owen, E. J. Rhodes, and J. Q. Spencer (2000), Timing of Late Quaternary glaciations south of Mount Everest in the Khumbu Himal, Nepal, *Geol. Soc. Am. Bull.*, *112*(10), 1621–1632.
Richards, B. W. M., L. A. Owen, and E. J. Rhodes (2001), Asynchronous glaciation at Nanga Parbat, northwestern Himalaya Mountains, Pakistan: Comment, *Geology*, *29*(3), 287.
Roe, G. H., D. R. Montgomery, and B. Hallet (2002), Effects of orographic precipitation variations on the concavity of steady-state river profiles, *Geology*, *30*(2), 143–146.
Roe, G. H., D. R. Montgomery, and B. Hallet (2003), Orographic precipitation and the relief of mountain ranges, *J. Geophys. Res.*, *108*(B6), 2315, doi:10.1029/2001JB001521.
Schneider, D. A., M. A. Edwards, W. S. F. Kidd, M. A. Khan, L. Seeber, and P. K. Zeitler (1999), Tectonics of Nanga Parbat, western Himalaya: Synkinematic plutonism within the doubly vergent shear zones of a crustal-scale pop-up structure, *Geology*, *27*(11), 999–1002.
Sklar, L., and W. E. Dietrich (1998), River longitudinal profiles and bedrock incision models: Stream power and the influence of sediment supply, in *Rivers Over Rock: Fluvial Processes in Bedrock Channels*, *Geophys. Monogr. Ser.*., vol. 107, edited by K. J. Tinkler and E. E. Wohl, pp. 237–260, AGU, Washington, D. C.
Snyder, N. P., K. X. Whipple, G. E. Tucker, and D. J. Merritts (2000), Landscape response to tectonic forcing: DEM analysis of stream profiles in the Mendocino triple junction region, northern California, *Geol. Soc. Am. Bull.*, *112*(8), 1250–1263.
Snyder, N. P., K. X. Whipple, G. E. Tucker, and D. J. Merritts (2003), The importance of a stochastic distribution of floods and erosion thresholds in the bedrock river incision problem, *J. Geophys. Res.*, *108*(B2), 2117, doi:10.1029/2001JB001655.
Strahler, A. N. (1952), Hypsometric (area-altitude) analysis of erosional topography, *Geol. Soc. Am. Bull.*, *63*, 1117–1141.
Sugden, D. E., and B. S. John (1976), *Glaciers and Landscape*, 376 pp., Arnold, London.
Suggate, R. P. (1990), Late Pliocene and Quaternary glaciations of New Zealand, *Quat. Sci. Rev.*, *9*, 175–197.
Thiede, R. C., B. Bookhagen, J. R. Arrowsmith, E. R. Sobel, and M. R. Strecker (2004), Climatic control on rapid exhumation along the southern Himalayan Front, *Earth Planet. Sci. Lett.*, *222*, 791–806.
Tippett, J. M., and P. J. J. Kamp (1993), Fission track analysis of the Late Cenozoic vertical kinematics of continental Pacific crust, South Island, New Zealand, *J. Geophys. Res.*, *98*(B9), 16,119–16,148.
Tomkin, J. H. (2003), Erosional feedbacks and the oscillation of ice masses, *J. Geophys. Res.*, *108*(B10), 2488, doi:10.1029/2002JB002087.
Tomkin, J. H. (2007), Coupling glacial erosion and tectonics at active orogens: A numerical modelling study, *J. Geophys. Res.*, *112*, F02015, doi:10.1029/2005JF000332.
Tomkin, J. H., and J. Braun (2002), The influence of alpine glaciation on the relief of tectonically active mountain belts, *Am. J. Sci.*, *302*, 169–190.
Tucker, G. E., and R. L. Bras (1998), Hillslope processes, drainage density, and landscape morphology, *Water Resour. Res.*, *34*, 2751–2764.
Tucker, G. E., and R. L. Slingerland (1994), Erosional dynamics, flexural isostasy, and long-lived escarpments: A numerical modeling study, *J. Geophys. Res.*, *99*(B6), 12,229–12,243.
Tucker, G. E., and K. X. Whipple (2002), Topographic outcomes predicted by stream erosion models: Sensitivity analysis and intermodel comparison, *J. Geophys. Res.*, *107*(B9), 2179, doi:10.1029/2001JB000162.
Walcott, R. I. (1998), Modes of oblique compression: Late Cenozoic tectonics of the South Island of New Zealand, *Rev. Geophys.*, *36*, 1–26.
Whipple, K. X. (2004), Bedrock rivers and the geomorphology of active orogens, *Ann. Rev. Earth Planet. Sci.*, *32*, 85–151.
Whipple, K. X., and S. H. Brocklehurst (2000), Estimating glacial relief production in the Nepal Himalaya, *Geol. Soc. Am. Abstr. Programs*, *32*, A320.
Whipple, K. X., and B. J. Meade (2004), Controls on the strength of coupling among climate, erosion, and deformation in two-sided, frictional orogenic wedges at steady state, *J. Geophys. Res.*, *109*, F01011, doi:10.1029/2003JF000019.
Whipple, K. X., E. Kirby, and S. H. Brocklehurst (1999), Geomorphic limits to climate-induced increases in topographic relief, *Nature*, *401*, 39–43.
Willett, S. D. (1999), Orogeny and orography: The effects of erosion on the structure of mountain belts, *J. Geophys. Res.*, *104*(B12), 28,957–28,981.
Wobus, C. W., K. V. Hodges, and K. X. Whipple (2003), Has focused denudation sustained active thrusting at the Himalayan topographic front?, *Geology*, *31*(10), 861–864.
Wobus, C. W., K. X. Whipple, E. Kirby, N. P. Snyder, J. Johnson, K. Spyropolou, B. Crosby, and D. Sheehan (2006), Tectonics from topography: Procedures, promise and pitfalls, in *Tectonics, Climate and Landscape Evolution*, edited by S. D. Willett et al., *Spec. Pap. Geol. Soc. Am.*, *398*, 55–74.
Zeitler, P. K. (1985), Cooling history of the NW Himalaya, Pakistan, *Tectonics*, *4*(1), 127–151.
Zeitler, P. K., et al. (2001), Erosion, Himalayan geodynamics, and the geomorphology of metamorphism, *GSA Today*, *11*(1), 4–9.

S. H. Brocklehurst, School of Earth, Atmospheric and Environmental Sciences, University of Manchester, Manchester M13 9PL, UK. (shb@manchester.ac.uk)
K. X. Whipple, School of Earth and Space Exploration, Arizona State University, Tempe, AZ, USA.